DOI: 10.1002/chem.200501390

Lanthanide Complexes of a Picolinate Ligand Derived from 1,4,7-Triazacyclononane with Potential Application in Magnetic Resonance Imaging and Time-Resolved Luminescence Imaging

Aline Nonat, Christelle Gateau, Pascal H. Fries, and Marinella Mazzanti*[a]

Abstract: The new potentially octadentate ligand, 1-(carboxymethyl)-4,7-bis[(6-carboxypyridin-2-yl)methyl]-1,4,7-triazacyclononane (H_3bpatcn), in which two picolinate arms and one acetate arm are connected to the 1,4,7-triazacyclonane core, has been prepared. Potentiometric studies show an increased stability of the Gd^{III} complex of H_3bpatcn ($\log K_{GdL} = 15.8(2)$) with respect to the Gd^{III} complex of the analogous ligand 1,4,7-triazacyclononane-*N*,*N*′,*N*″-triacetic acid (H_3nota) ($\log K_{GdL} = 13.7$), associated with an increased selectivity of H_3bpatcn for gadolinium over calcium. The H_3bpatcn ligand sensitises the terbium ion very efficiently, leading to a long-lived and highly luminescent terbium complex (quantum yield = 43%), in spite of the presence of a coordinated water molecule. ^{1}H proton NMR studies indicate that the metal ion is rigidly encapsulated by the three arms of the octadentate ligand H_3bpatcn and that the macrocycle framework remains bound (through the five nitrogen and the three oxygen atoms) even at high temperature. A new theoretical method for interpreting the water proton relaxivity is presented. It is based on recent progresses in the description of the electronic spin relaxation and on an auxiliary probe solute. It replaces the Solomon, Bloembergen and Morgan (SBM) framework, which is questionable at low field, while avoiding resorting to simulations and/or sophisticated theories with additional unknown zero-field splitting (ZFS) parameters. The inclusion of two picolinate groups on a triazacyclononane framework affords the mono-aquo gadolinium complex [Gd(bpatcn)(H_2O)] with favourable electron-relaxation properties ($\tau_{S0}^{eff} = 125$ ps). The optimisation of the electronic relaxation by ligand design is especially important to achieve high relaxivity in the new generation macromolecular complexes with long rotational correlation times.

Keywords: gadolinium · luminescence · N ligands · relaxometry · terbium

Introduction

The unique spectroscopic and magnetic properties of lanthanide ions have allowed for the use of their complexes in a wide range of medical and biochemical applications. The high magnetic moment ($S = 7/2$) and the slow electronic relaxation of gadolinium make it ideal for the design of magnetic resonance imaging (MRI) relaxation agents,[1–7] while the long-lived luminescence of Eu^{III} and Tb^{III} complexes has been exploited in the development of sensors, time-resolved high-throughput assays and fluorescence imaging.[8–12] The ligand design is crucial for the effective use of the lanthanide properties in such biomedical applications and has incited a large number of coordination chemistry studies.[1,4,13–16] Poly(amino)carboxylates ligands have been particularly investigated, since the high thermodynamic and kinetic stability often found in their complexes are essential features to prevent in vivo toxicity. All current Gd^{III}-based commercial contrast agents are low-molecular-weight complexes of octadentate poly(aminocarboxylate) ligands such as the macrocyclic H_4dota (1,4,7,10-tetraazacyclododecane-*N*,*N*′,*N*″,*N*‴-tetraacetic acid), and the acyclic H_5dtpa (diethylenetriamine-*N*,*N*′,*N*″-pentaacetic acid).[2] In these complexes the relaxivity (the key property of a contrast agent expressing its ability to enhance the relaxation rate of the solvent water protons) is much lower than the theoretical maximum, due to a lack of simultaneous optimisation of all the parameters determining the relaxation enhancement.

[a] A. Nonat, Dr. C. Gateau, Dr. P. H. Fries, Dr. M. Mazzanti
Laboratoire de Reconnaissance Ionique
Service de Chimie Inorganique et Biologique (UMR-E 3 CEA-UJF)
CEA/DSM/Département de Recherche Fondamentale
sur la Matière Condensée
CEA-Grenoble, 38054 Grenoble cedex 09 (France)
Fax: (+33) 438-785-090
E-mail: mazzanti@drfmc.ceng.cea.fr

Supporting information for this article is available on the WWW under http://www.chemeurj.org/ or from the author.

Higher relaxivity is required for the next generation of target-specific MRI contrast agents.[17] High relaxivity can be obtained in the presence of a high number of inner-sphere water molecules allied with an optimised water-exchange rate, a long rotational correlation time and a long electronic relaxation time.[5,18] Though large efforts have been devoted to the understanding of the molecular parameters that govern the relaxivity, the mechanisms and the coordination properties underlying the electronic relaxation of Gd^{III} complexes still remain poorly understood.[19–22] This prevents the ligand design required to optimise the electronic relaxation, which becomes especially important in the new generation macromolecular complexes with long rotational correlation times.

Recently, we reported gadolinium complexes of tripodal or tetrapodal ligands containing picolinate arms showing interesting relaxation properties.[23–27]

The tetrapodal ligand *N*,*N*′-bis[(6-carboxypyridin-2-yl)-methyl]-ethylenediamine-*N*,*N*′-diacetic acid (H_4bpeda) yields soluble nonacoordinated complexes of gadolinium with one water molecule bound to the gadolinium ion. This complex shows water proton relaxivity and water-exchange rates similar (or slightly favourable) to commercial contrast agents. The NMRD profile[28] and multifrequency EPR studies of this complex showed a rapid electron-spin relaxation below 1 T. At 0.34 T, $[Gd(bpeda)(H_2O)]^-$ was found to be among the Gd^{3+} complexes having the fastest transverse electronic relaxation to date.[25] Dramatically different relaxation properties were observed for the highly symmetric nonadentate ligand 1,4,7-tris[(6-carboxypyridin-2-yl)methyl]-1,4,7-triazacyclononane (H_3tpatcn), which contains three picolinate arms connected to the 1,4,7-triazacyclonane core. H_3tpatcn yields a highly rigid nonacoordinated gadolinium complex that does not contain coordinated water molecules and displays a particularly high relaxivity at low field <1 MHz (5.3 $mM^{-1}\,s^{-1}$ at 0.02 MHz and 298 K). A slow electron-spin relaxation was estimated from the NMRD profile of [Gd(tpatcn)][26] in agreement with detailed EPR studies on this complex; the EPR spectra display the smallest peak-to-peak widths observed for gadolinium chelates (at 0.34 T and at room temperature $\Delta H_{pp}=15$ G).[29] The electron-spin relaxation of this complex was also determined by a new model-independent theory developed very recently in our laboratory.[27] The obtained value at zero field (~1500 ps) is the longest value reported to date (650 ps for dota). The remarkably slow electron relaxation of this complex has been interpreted in terms of the unusual coordination sphere containing six N donors associated to the complex C_3 symmetry.

To further investigate the influence of the coordination sphere on the electronic relaxation and to increase the relaxivity, we have prepared an analogous Gd^{III} complex containing one coordinated water molecule using the new ligand 1-(carboxymethyl)-4,7-bis[(6-carboxypyridin-2-yl)-methyl]-1,4,7-triazacyclononane (H_3bpatcn). In H_3bpatcn two picolinate arms and one acetate arm are connected to the 1,4,7-triazacyclonane core yielding a potentially octadentate ligand. Here we report the characterisation, the thermodynamic stability of the lanthanide complexes of this ligand and the relaxation properties of the gadolinium complex of $bpatcn^{3-}$. We also describe the photophysical properties of the terbium and europium complexes of the H_3bpatcn ligand. Picolinate groups are efficient sensitisers of lanthanide luminescence and their introduction in a decadentate ligand has previously yielded water-stable and highly luminescent terbium complexes.[30] In spite of the presence of a coordinated water molecule, usually leading to deactivation of the lanthanide emission, the terbium complex of $bpatcn^{3-}$ shows an intense and long-lived luminescence.

Results and Discussion

Synthesis and molecular structure of the ligand H_3bpatcn: 1-(Carboxymethyl)-4,7-bis[(6-carboxypyridin-2-yl)methyl]-1,4,7-triazacyclononane (H_3bpatcn) was obtained in three steps by using the synthetic route detailed in Scheme 1 with a global yield of 9% from the previously described 6-chloromethylpyridine-2-carboxylic acid ethyl ester. The reaction of 1,4,7-triazacyclononane trihydrochloride with two equivalents of 6-chloromethylpyridine-2-carboxylic acid ethyl ester in presence of K_2CO_3 produces a mixture of the desired disubstituted species (yield 24%), of a monosubstituted species (11%) and of the previously described trisubstituted spe-

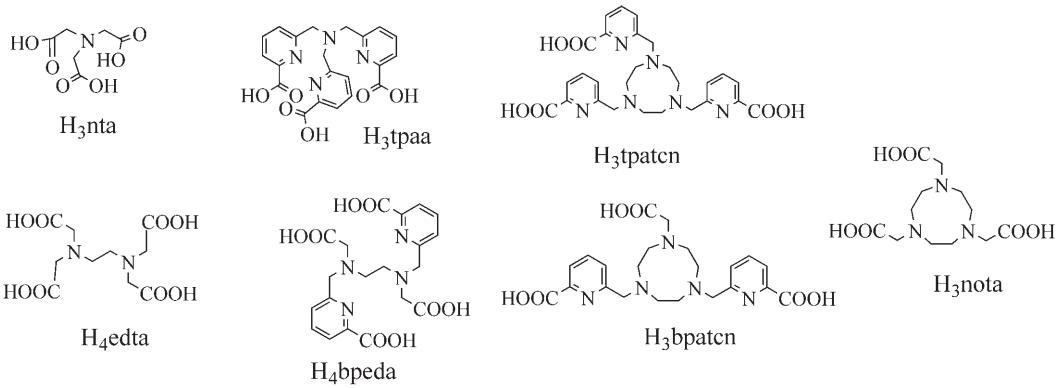

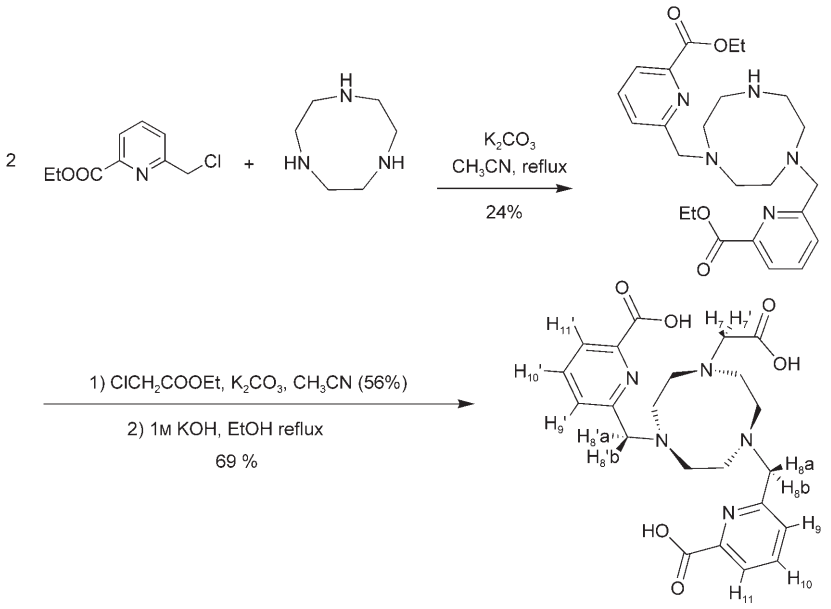

Scheme 1. Synthesis of the ligand H_3bpatcn and its numbering scheme for NMR spectral assignement.

cies[26] (yield 36%), which were separated by column chromatography. Reaction of the disubstituted product (1,4-bis[(6-carbethoxypyridin-2-yl)methyl]-1,4,7-triazacyclononane) with ethyl chloroacetate and K_2CO_3 followed by saponification produces, after adjustement of the pH (1.5), the ligand $(H_5bpatcn)Cl_2$ in its pentaprotonated form. The proton NMR spectra show all the expected resonances and satisfactory elemental analytical data were obtained.

The ^{1}H NMR spectrum of H_3bpatcn in D_2O at pD = 6.4 displays a single set of seven signals implying C_2 symmetry. The ethylene moiety of tacn gives rise to two peaks at δ = 3.53 and 3.58 ppm. The CH_2 protons close to the picolinate and the acetate groups appear as sharp single peaks at δ = 4.50 ppm and 3.83 ppm respectively. Pyridinic protons afford two doublets (δ = 7.58 ppm and 7.86 ppm) and a triplet (δ = 7.96 ppm). Crystals of H_3bpatcn·2 HCl·4 H_2O were obtained by slow evaporation of a concentrated water solution of the ligand at pH ~1.5. The structure is represented in Figure 1. The structure shows that all the three carboxylates are protonated with C–OH distances ranging from 1.201(4) to 1.215(4) Å. From the difference Fourier electron density map, the two remaining protons were found to be located on the two amino nitrogens of the macrocycle neighbouring the picolinate groups.

NMR spectroscopic studies: NMR spectroscopic studies on the complexes [Ln(bpatcn)] (Ln = La, Eu, Lu) have been carried out and compared with the similar studies reported for $[Ln(dota)]^-$ complexes and with studies on lanthanide complexes of ligands containing the 1,4,7-triazacyclononane macrocyclic core. Numerous studies of the solution behaviour of lanthanide complexes of polyaminocarboxylate ligands by variable-temperature NMR spectroscopy have been reported in the literature.[5] Conformational equilibria that interconvert different stereoisomers and coordination equilibria have been evidenced for the lanthanide complexes of dota and its derivatives.[31–35] The lanthanide complexes of the ligand $bpatcn^{3-}$ are expected to give rise to 24 signals in the proton NMR spectrum when coordination of all donor atoms takes place (C_1 symmetry). The rigid coordination of the lanthanide ions can result in two structurally independent elements of chirality associated with the coordinated triazamacrocycle and the torsion angles of the bound pendant arms. The ring can adopt two enantiomeric conformations (λλλ and δδδ) and the chelating arms

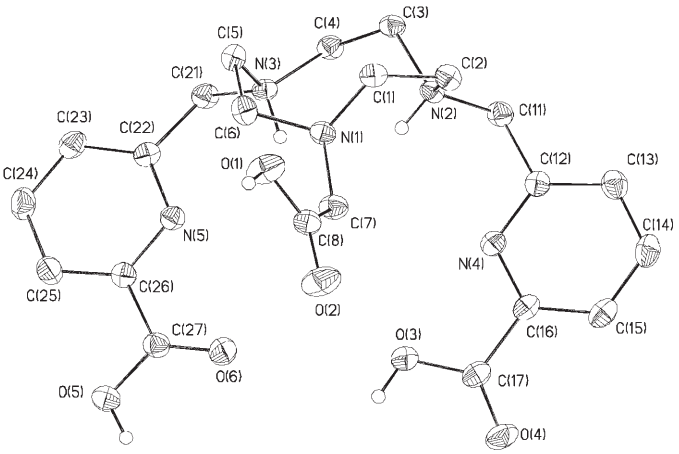

Figure 1. ORTEP diagram of the ligand $(H_5bpatcn)Cl_2·H_2O$, with 30% thermal contours for all atoms.

could be arranged in either a clockwise (Δ) or anticlockwise (Λ) helical fashion. Accordingly, two enantiomeric pairs (Λ-(λλλ)/Δ(δδδ) or Λ(δδδ)/Δ(λλλ)) of diastereoisomers could be formed and interconversion through ring inversion or concerted arm rotation could occur (Figure 2). The presence of two pairs of diastereoisomers with a rigid solution structure is expected to give rise to two sets of 24 ^{1}H NMR signals, while the presence of a rapid exchange between enantiomers would result in average C_s symmetric solution species yielding only 12 NMR signals. Arrangement of the chelating arms in a nonhelical fashion could probably also occur in these asymmetric complexes and would also result in C_1 symmetric isomers. Previous NMR studies on lanthanide complexes of the trianionic hexadentate triaza ligand 1,4,7-triazacyclononane-*N*,*N*′,*N*″-triacetic acid (H_4nota)[36] in water and those of the neutral hexadentate ligand 1,4,7-tris-

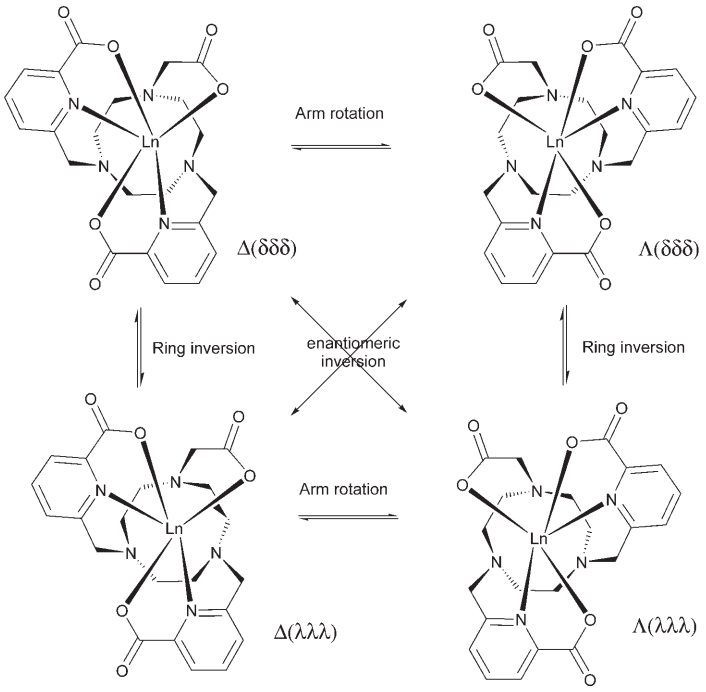

Figure 2. Schematic representation of the possible exchange mechanisms of the conformational isomers of [Ln(bpatcn)].

(carbamoylmethyl)-1,4,7-triazacyclononane[37] in acetonitrile suggested the presence in these complexes of a flexible triaza core with a fast interconversion between the two staggered conformations of the five-membered chelate rings M-N-C-C-N occurring in conjuction with the change of the pendant arm orientation. Conversely proton NMR studies of the complexes [Ln(tpatcn)] (Ln = Nd, Eu, Lu) indicate the absence of dynamic processes even at high temperature, with the metal remaining encapsulated in a rigid structure by the triazacyclononane ring and by the three arms of the ligand.[26]

The proton NMR of the lanthanum complex of bpatcn^{3-} in D_2O at pD = 7.1 and at 298 K at 400 MHz (Figure 3) shows three signals for the pyridine protons, two signals (doublets) for the diastereotopic methylene protons close to the pyridine, one resonance for the protons of the acetate group and three broad peaks for the protons of ethylene moiety of the macrocycle. Six narrow signals are expected at coalescence for the ethylene protons of the macrocycle in the presence of dynamically averaged C_s symmetric species in which the two picolinate pendant arms are equivalent. At 343 K four slightly broad peaks are observed for the ethylene moiety of the macrocycle indicating that coalescence is not yet fully achieved at this temperature. The diastereotopic character of the CH_2 close to the pyridine is expected in the presence of a long-lived coordination of the three ligand arms to the metal on the NMR timescale. The inversion of the macrocyclic ring associated to the concerted rotation of the three carboxylate groups generate a symmetry plane passing through the acetate arm and the metal ion; this symmetry gives rise to a single peak for the two acetate protons.

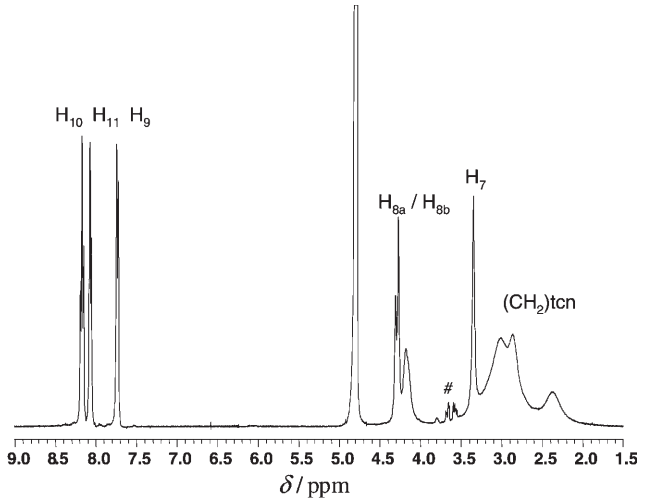

Figure 3. ^{1}H NMR spectrum at 298 K of [La(bpatcn)] in D_2O at pD = 7.1 (# denotes a hydrolite impurity).

The observed spectral features can therefore be interpreted in terms of a fast interconversion between two conformational enantiomers (Λ(λλλ)/Δ(δδδ) or Λ(δδδ)/Δ(λλλ), Figure 2) yielding a dynamically averaged C_s symmetry. The proton NMR spectra in water, in the range 298–278 K, and in a water/methanol mixture, in the range 278–233 K, show only increasingly broader peaks. This indicates that an exchange process is slowed down in this temperature range. The slow exchange limit of the process interconverting enantiomeric pairs is expected to give rise to 24 NMR signals.

At 343 K, the proton NMR spectrum of the Eu^{III} complex of bpatcn^{3-} in D_2O solution at pD = 9.1 (Figure 4) shows only one set of 24 narrow signals of equal intensity with six resonances for the pyridine protons, twelve resonances for

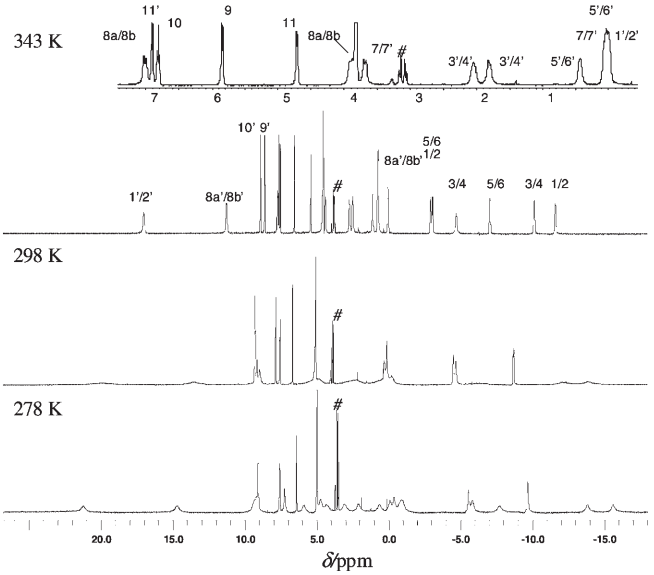

Figure 4. ^{1}H NMR spectra of [Eu(mabpatcn)] in D_2O at pD = 9.1 (# denotes a hydrolite impurity).

the protons of the ethylenic moiety (six axial and six equatorial) of the macrocycle and six resonances for the methylene protons of the pendant arms. These features are in agreement with the presence of C_1 symmetric species at this temperature in which the three macrocyclic nitrogen atoms and the three ligand arms remain coordinated to the metal on the NMR timescale.[38–40] The signals were completely attributed by a 2D-COSY experiment combined with a ^{1}H-^{1}H NOESY experiment. A two-dimensional EXSY experiment performed at 343 K showed 12 cross peaks between two symmetry-related sets of protons indicating the presence of an exchange between conformational isomers. This can be interpreted by the presence in solution of one pair of enantiomers (Λ(λλλ)/Δ(δδδ) or Λ(δδδ)/Δ(λλλ)) in slow exchange at this temperature. Upon lowering the temperature the proton NMR spectrum of the [Eu(bpatcn)(H_2O)] complex undergoes a severe broadening indicating that a second dynamic process is slowed down. Below 283 K the signals become narrower and the spectrum at 278 K is similar to the one at 343 K showing 24 signals, but broader and slightly shifted (Figure 4). This complex dynamic behaviour could be accounted for by an exchange process between isomers present in solution at very different concentration and involving only arm rotation or ring inversion. The low concentration of the minor isomer (which would give rise to a second set of 24 signals) prevents its identification at 278 K. A similar unusual dynamic behaviour has been previously observed for a dota^{4-} derivative containing a *p*-nitrophenyl substituent[41] and interpreted in terms of an exchange process involving one major species and at least one minor isomer of very low concentration the relative population of which changes with temperature.

The ^{1}H NMR spectrum of the diamagnetic Lu^{III} complex of bpatcn^{3-} in D_2O solution at pD = 4.2 at 298 K (Figure 5)

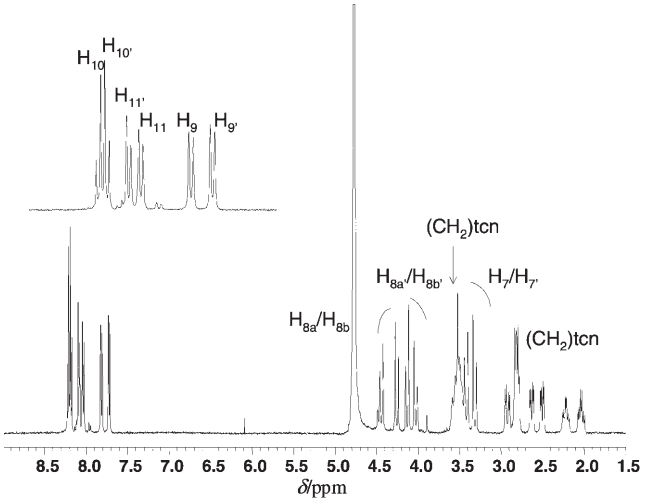

Figure 5. ^{1}H NMR spectrum at 298 K of [Lu(bpatcn)] in D_2O at pD = 4.2.

shows only one set of 24 signals, with six resonances for the pyridine protons, twelve resonances partially overlapped for the protons of the ethylene moiety (six axial and six equatorial) of the macrocycle and six resonances for the diastereotopic methylene protons of the pendant arms. A 2D-COSY experiment combined with a ^{1}H-^{1}H NOESY experiment allowed the accurate assignment of the pyridine protons and of the methylene protons of the pendant arms. A strong NOE effect is observed between the protons $H_{8a/8b}$ and $H_{8a'/8b'}$ of the CH_2 group close to the pyridine and the pyridine protons H_9 and $H_{9'}$. The CH_2–CH_2 moieties of the macrocycle form a complex series of multiplets, doublets of doublets and triplets that were only partially assigned. These features are consistent with the presence of a highly rigid C_1 symmetric solution structure in which the macrocyclic framework and the pendant arms remain bound and rigid on the NMR timescale. The proton NMR spectra remain unchanged in the pD range 4.2–9. A very similar ^{1}H NMR spectrum (Figure S1 in the Supporting Information) showing high conformational rigidity was observed for the yttrium complex (the Y^{III} ion has a coordination number and ionic radius similar to the Er^{III} ion).

Two-dimensional EXSY experiments were performed in water at 298 and 343 K. While no exchange was detected at room temperature, at 343 K the two-dimensional EXSY spectrum in water features cross peaks associated with the slow exchange of the two groups of protons (1–11 and 1′-11′) located in the opposite sides of a symmetry plane arising from the slow interconversion between two pair of C_1 symmetric enantiomers (Λ(λλλ)/Δ(δδδ) or Λ(δδδ)/Δ(λλλ)). The ^{1}H NMR spectra recorded in D_2O between 278 and 298 K show a splitting pattern almost unchanged over this temperature range, indicating the absence of a second dynamic process in this range.

While an exchange between two enantiomeric pairs is observed at elevated temperature for the La^{III} and the Lu^{III} complexes of dota^{4-}, a very different behaviour is found for the [La(bpatcn)] and [Lu(bpatcn)) complexes with an increased rigidity observed for the smaller lanthanide ions (Y^{III} and Lu^{III} complexes).

These results suggest that the lanthanide ions are encapsulated by the three arms of bpatcn^{3-} and that the macrocycle framework remains bound by the five nitrogen and the three oxygen atoms, even at high temperature, as previously observed for the lanthanide complexes of the symmetric nonadentate ligand tpatcn.[26] Moreover, on the basis of the NMR studies, a similar arrangement of the donor atoms around the metal centre can be anticipated for the lanthanide complexes of tpatcn^{3-} and bpatcn^{3-}.

Proton NMR studies had allowed to evidence the conformational rigidity of a nonadentate derivative of 1,4,7-triazacyclononane with three iminocarboxylic pendant arms.[42] The Schröder group reported recently the solid-state and solution structure of the lanthanide complexes [Ln(L)-(CH_3COO)] of an analogous heptadentate bisanionic derivative 1,4,7-triazacyclononane with two iminocarboxylic pendant arms.[43] While a more flexible solution structure is observed for the yttrium complex of this ligand, the solid-state coordination geometries of the two series are similar. This is a consequence of the presence of the 1,4,7 triazacyclono-

nane capping group, which forces the Ln ion to assume a trigonal prismatic structure.

Finally, the replacement of one bidentate pyridinecarboxylate arm in the ligand tpatcn^{3-} with a monodentate acetate to produce bpatcn^{3-} does not result in a significant modification of the coordination mode or in an increased fluxionality for complexes of smaller lanthanide ions. An increased conformational mobility is, however, found for the larger lanthanide ions.

Protonation constants and stability constants: The deprotonation constants of H_3bpatcn defined as $K_{ai} = [H_{6-i}L]^{3-i}/[H_{5-i}L]^{2-i}[H]^+$ were determined to be $pK_{a1} = 2.2(2)$, $pK_{a2} = 2.3(2)$, $pK_{a3} = 3.7(3)$, $pK_{a4} = 5.42(3)$ and $pK_{a5} = 10.5(2)$ (0.1 M KCl, 298 K) by potentiometric titration. The titration curves of H_3bpatcn and of its Gd^{III} and Ca^{II} complexes are shown in Figure S2 in the Supporting Information. Variable pH proton NMR spectroscopy of the ligand shows significant variations (0.3–0.4 ppm) in the chemical shift of both types of methylene protons (close to the picolinic or to the carboxylic acid) during the fifth (pH 10–13) and fourth protonation processes (pH 4,5–7). Significant variations are observed only for the methylene protons close to the picolinic group during the second and third protonation processes (pH 1.5–4.5). Significant variations are observed also for the chemical shifts of the three pyridyl protons (H3 and to a lesser extent H4 and H5, 0.3–0.2 ppm) upon the second and third protonation processes. The protonation curves indicate that the first two equivalents of acid protonate equally the different type of nitrogen atoms of the macrocycle ($pKa_4 = 5.42(3)$, $pKa_5 = 10.5(2)$). The next two equivalents protonate the carboxylates bound to the pyridines ($pK_{a2} = 2.3(2)$, $pK_{a3} = 3.71(3)$). The value of pK_{a1} (2.2(2)) is consistent with the value found for the protonation of the carboxylate in H_3nota ligand (2.88(2)).[36] The crystal structure of the protonated ligand H_3bpatcn·2HCl isolated at pH ~2, showing that all carboxylic acid oxygen atoms and the two macrocycle nitrogen atoms (adjacent to the picolinates) are protonated, is also in agreement with the assignment of the pK_{a1} to the protonation of the carboxylic acid. The protonation curve and the structural data are in agreement with a simultaneous partial protonation of the three macrocycle nitrogens, as previously observed for the ligand H_3nota, followed by the protonation of the carboxylate groups. The protonation of the third amine and of the pyridine nitrogens occur at lower pH and the associate pK_a could not be determined. The two highest pK_a's are very similar to the highest pK_a's of the cyclic triamine 1,4,7-triazacyclononane (10.42, 6.82)[44] and of the macrocyclic triaza ligand H_3nota (11.3(1) and 5.59(2)). The values of pK_{a2} and pK_{a3} are consistent with the values found for the protonation of the picolinate groups in the tripodal ligand H_3tpaa (H_3tpaa = α,α′,α″-nitrilotri(6-methyl-2-pyridinecarboxylic acid) ($pK_{a2} = 3.3(1)$, $pK_{a3} = 4.11(6)$).[24] While the introduction of pyridinecarboxylate groups results in the decrease of the overall basicity of the ligand H_3tpaa with respect to H_3nta (nitrilotriethanoic acid) and of the ligand H_4bpeda with respect to H_4edta,[25] the H_3bpatcn ligand has a protonation scheme and pK_a values very similar to his parent ligand H_3nota (Table 1).

Table 1. Values of pK_a and $\log K$ for H_4bpdea and related ligands.

Ligand	pK_a	$\log K_{GdL}$	$\log K_{CaL}$
H_3bpatcn[a]	10.5(2),5.42(3),3.71(3),2.3(2),2.2(2)	15.8(2)	8.18(7)
H_3nota[b]	11.3,5.6,2.88	13.7	8.92
H_4bpdea[c]	8.5(1),5.2(2),3.5(1),2.9(1)	15.1(3)	9.4(1)
H_4edta[b]	10.19,6.13,2.69,2.60	17.4	10.5
H_3nta[b]	9.75,2.64,1.57	11.4	
H_3tpaa[d]	4.11(6),3.3(1),2.5(2)	10.2(2)	8.5(2)

[a] This work. [b] From reference [46], which does not include experimental errors. [c] From reference [25]. [d] From reference [24].

The stability constants of the complexes formed between Gd^{III} and Ca^{II} ions and H_3bpatcn have been determined by direct titration of 1:1 metal/H_3bpatcn (5×10^{-4} M) mixtures in the pH range 2.5–8.5. Titration data could be fitted to Equations (1) and (2).

$$Gd^{3+} + \text{bpatcn}^{3-} \rightleftharpoons [Gd(\text{bpatcn})] \quad \log K_{GdL} = 15.8(2) \qquad (1)$$

$$Ca^{2+} + \text{bpatcn}^{3-} \rightleftharpoons [Ca(\text{bpatcn})]^- \quad \log K_{CaL} = 8.18(7) \qquad (2)$$

The values of pGd = 13.6 and pCa = 6.30 ($-\log[M]_{free}$ at pH 7.4, $[M]_{total} = 1$ μM and $[\text{bpatcn}]_{total} = 10$ μM), which allow a straightforward comparison of complex stabilities in physiological conditions, suggest a quite good physiological stability with respect to the commercial contrast agent [Gd(dtpa-bma)(H_2O)]$^-$ ($\log K_{GdL} = 16.85$, pGd = 15.8, pCa = 6.39) although probably too low for in vivo application.[45,46]

While the pK_a values and therefore the basicity of H_3bpatcn and H_3nota are very similar, the stability of the gadolinium complex of bpatcn^{3-} is significantly higher than that of the nota complex ($\log K_{GdL} = 13.7$).[36] The presence of the two additional N-donor atoms provided by the pyridyl groups in bpatcn results in an increased stability (2.1 log units) of the gadolinium complex. The contribution of the 2-pyridylmethyl to stability was evaluated to 2.6 log units for the cation Gd^{III} complex of the edta derivative *N*,*N*′-bis(2-pyridinylmethyl)ethylenediamine-*N*,*N*′-diacetate.[47] However, in our previous studies we observed that in spite of the presence of two (bpeda^{4-} with respect to the ligand edta^{4-}) or three (tpaa^{3-} with respect to nta^{3-}) additional coordinating pyridyl nitrogen atoms, the stability of the gadolinium complex and of the calcium complex is lower for the octadentate ligand bpeda^{4-} with respect to hexadentate edta^{4-} and for heptadentate ligand tpaa^{3-} with respect to the tetradentate nta^{3-}(Table 1). The decrease in stability was explained in terms of the decreased overall basicity of the ligands containing 6-methyl-2-pyridinecarboxylic, leading to the conclusion that the pyridine does not contribute significantly to the complex stability when included in the 6-methyl-2-pyridinecarboxylic group.[25] The results presented here show that if the ligand basicity is maintained the pyri-

dine N-donor groups contribute significantly to the stability of the gadolinium complex even when included in the 6-methyl-2-pyridinecarboxylic group. Moreover the stability constant of the calcium complex of bpatcn^{3-} is approximately the same of that of nota^{3-}. Hence, the pyridyl goups in bpatcn^{3-} produce a selectivity for Gd^{III} over Ca^{II}. High selectivity of the ligand for gadolinium over physiological metals is crucial for the application of its complexes in MRI, since the release of Gd^{III} associated to transmetallation in vivo is responsible for the toxicity of gadolinium complexes.[48]

Photophysical properties: The photophysical properties of lanthanides (sharp emission, long luminescence lifetime allowing to discriminate between the background fluorescence of biological materials and the target signal) make their complexes very attractive for the application as luminescent labels in time-resolved imaging and in biomedical assays.[1,9,11,49] In spite of numerous studies directed to prepare highly luminescent complexes, the lanthanide-based, commercial luminescent labels remain scarce,[50] due to the high requirements on the design of suitable labels. The preparation of lanthanide complexes that are stable and highly emissive in water requires the design of polydentate ligands that contain suitable sensitisers of the lanthanide emission, capable of shielding the metal centre from the solvent water molecules to prevent nonradiative deactivation of the lanthanide excited states by O–H oscillators. We have recently reported that the incorporation of picolinate groups in a decadentate ligand yields highly luminescent terbium and europium complexes.[25] These results incited the study of the photophysical properties of the terbium and europium complexes of bpatcn^{3-}. The solvation state of the bpatcn^{3-} complexes of Eu and Tb was studied by comparison of their luminescence decays in H_2O and D_2O. Due to the different quenching efficiencies of the O–H and O–D oscillators, the measurement of Ln^{3+} phosphorescence lifetimes (τ) in H_2O and D_2O allows an accurate estimation of the number of coordinated water molecules present in solution (q) by using the equation of Beeby and co-workers ($q = A_{Ln}(1/\tau_{H_2O} - 1/\tau_{D_2O} - \alpha_{Ln})$ with $A_{Tb} = 5$ ms, $A_{Eu} = 1.2$ ms, $\alpha_{Tb} = 0.06$ ms^{-1} and $\alpha_{Eu} = 0.25$ ms^{-1}),[51] (a corrected version of the empirical equation of Horrocks and Sudnick[52] accounting for closely diffusing OH oscillators). The observed lifetimes of the Eu($^5D_0$) ($\tau_{H_2O} = 0.542(4)$ ms and $\tau_{D_2O} = 1.67(4)$ ms) and Tb ($^5D_4$) ($\tau_{H_2O} = 1.49(2)$ ms and $\tau_{D_2O} = 2.46(7)$ ms) levels for the [Tb(bpatcn)$(H_2O)_x$] and [Eu(bpatcn)$(H_2O)_x$] complexes are in agreement with the presence of $x = 1.2 \pm 0.2$ and 1.0 ± 0.2 coordinated water molecules in the Eu and Tb complexes, respectively. A similar number of coordinated water molecules can be expected for the gadolinium ion, which has a ionic radius intermediate between those of Eu and Tb.

The absorption spectra of bpatcn^{3-} and of its Eu^{III} and Tb^{III} complexes show an intense band at ~36500 cm^{-1} with a molar absorption coefficient of 9050 for Eu and of 9100 for Tb. These bands were assigned to a combination of $\pi \rightarrow \pi^*$ and $n \rightarrow \pi^*$ ligand-centred transitions.[53] The emission spectra of solutions of the europium and terbium complexes at pH 7.4 (obtained under excitation at 273 nm) show the usual $^5D_0 \rightarrow {}^7F_J$ and $^5D_4 \rightarrow {}^7F_J$ ($J = 0$–6) and transitions typical of the Eu^{3+} and Tb^{3+} ions, respectively (Figure 6). The luminescent properties of the visible-emitting lanthanide ions Eu and Tb are efficiently sensitised by the ligand bpatcn^{3-}. An efficient ligand-to-metal energy transfer is suggested by the close matching of the excitation and absorption spectra of the Tb chelates (Figure 7). The value of the sensitised emission quantum yield of the [Tb(bpatcn)(H_2O)] complex (ϕ = 43%) measured relative to $[Tb(dpa)_3]^{3-}$ (H_2dpa = dipicolinic acid) in aerated 0.1 M tris(hydroxymethyl)aminomethane (Tris) buffer with an experimental error of 15% is one of the highest reported to date[10,54–57] and the highest value found for terbium complexes containing a water molecule coordinated to the metal centre. The bpatcn^{3-} chromophore sensitises the Eu ion less efficiently, leading to a quantum

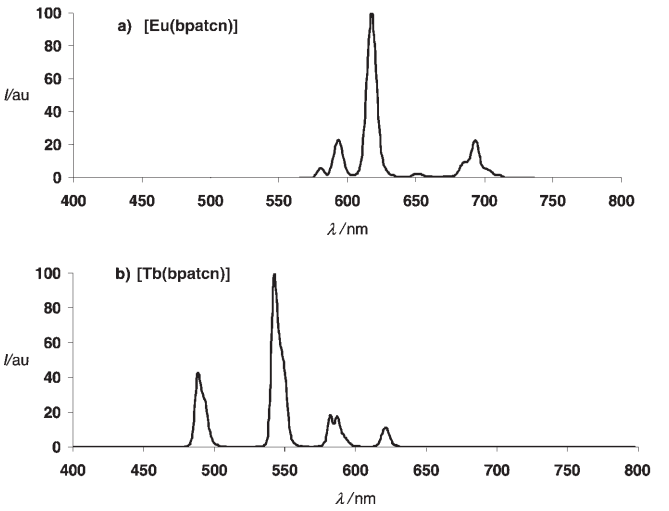

Figure 6. Normalised emission spectrum of a) [Eu(bpatcn)] and b) [Tb(bpatcn)] upon ligand excitation at 274 nm.

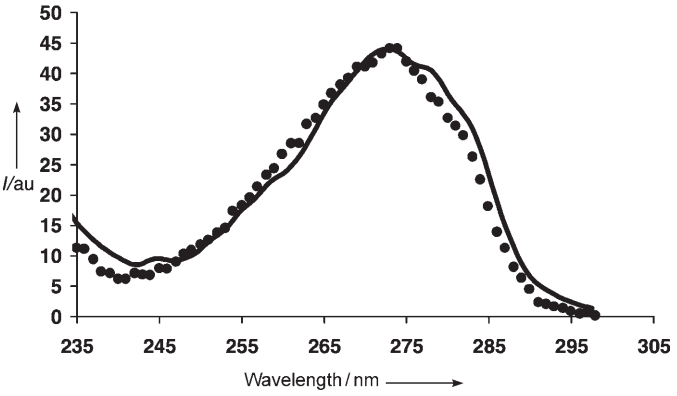

Figure 7. Absorption (·····) of H_3bpatcn and excitation spectrum (——) of [Tb(bpatcn)] in Tris buffer.

yield value $\phi = 5\,\%$, similar to the quantum yield of lanthanide-based commercial luminescent probes.[58,59] The very intense luminescence of the Tb ion is a result of efficient ligand-to-metal energy transfer and indicates an effective shielding of the metal ion from radiationless deactivation in spite of the presence of a water molecule coordinated to the metal. The long luminescence lifetime observed for the terbium complex in H_2O (1.5 ms) rules out the presence of a de-excitation pathway involving back-transfer from the excited state of the metal to the ligand. The low efficiency of this nonradiative decay process (the most important in terbium) results in a high luminescence quantum yield of the terbium complex. The comparison of the luminescence behaviour in water and deuterated water shows that the solvent-induced nonradiative decay process affects the quantum yield of the terbium complex to a lesser extent with respect to the europium complex (Table 2).

Table 2. Lifetime and absolute quantum yields in Tris buffer, pH 7.4 (298 K) relative to $[Eu(dpa)_3]^{3-}$ and $[Tb(dpa)_3]^{3-}$.

	λ_{exc} [nm]	ε [$M^{-1}cm^{-1}$]	τ_{H_2O} [ms]	τ_{D_2O} [ms]	ϕ_{H_2O}	ϕ_{D_2O}
bpatcn	272	7850				
[Eu(bpatcn)]	273	9050	0.542(4)	1.67(4)	0.05	0.12
[Tb(bpatcn)]	273	9100	1.49(2)	2.46(7)	0.43	0.48

Relaxivity theory: In an external field B_0, the efficiency of a Gd^{III} complex to enhance the contrast of T_1-weighted magnetic resonance (MR) images is gauged by its relaxivity[2,5] r_1, which is defined as the paramagnetic relaxation enhancement (PRE) of the longitudinal relaxation rate of the water protons due to a 1 mM increase of the concentration of this complex, also named (relaxation) contrast agent (CA). This definition readily extends to the protons of a solute. In the presence of a concentration [GdL] (mM) of paramagnetic GdL complexes, the measured longitudinal relaxation rate R_1 (s^{-1}) of nuclear spins I is the sum given[2,5] in Equation (3) of the relaxation rate R_{10} in the diamagnetic solution without Gd^{III} complexes and of the PRE R_{1p} of the spins I due to their interactions with the electronic spins S of the complexed Gd^{III} ions.

$$R_1 = R_{10} + R_{1p} \tag{3}$$

In Equation (4), the PRE R_{1p} is conveniently split into inner-sphere (IS) and outer-sphere (OS) contributions R_{1p}^{IS} and R_{1p}^{OS}.

$$R_{1p} = R_{1p}^{IS} + R_{1p}^{OS} \tag{4}$$

These contributions originate from two different starting situations of the random intermolecular trajectories of the water or solute molecule with respect to the gadolinium complex. At initial time $t = 0$, this species directly coordinates Gd^{III} in the case of the IS mechanism, whereas it undergoes a relative translational diffusion with respect to the complex for the OS contribution.

The (longitudinal) relaxivity r_1 ($s^{-1}mM^{-1}$) is expressed in Equation (5) as the sum of the IS and OS relaxivities $r_1^{IS} \equiv R_{1p}^{IS}/[GdL]$ and $r_1^{OS} \equiv R_{1p}^{OS}/[GdL]$.

$$r_1 \equiv \frac{R_{1p}}{[GdL]} = r_1^{IS} + r_1^{OS} \tag{5}$$

The popular Solomon, Bloembergen and Morgan (SBM) approach[2,5] provides a general expression of the IS relaxivity r_1^{IS} of the water protons. This expression depends on 1) the number (q) of coordinated water molecules, 2) the coordination lifetime (τ_M) of a water molecule and 3) the nuclear relaxation time (T_{1M}) of a water proton due to its magnetic dipole–dipole coupling, with the Gd^{III} spin in the limiting situation in which the water molecule bearing this proton would be coordinated to the metal for an infinite duration. Note that the theoretical nuclear relaxation rate $1/T_{1M}$ used in this work to calculate the IS relaxivity is different from the usual SBM expression. It is obtained by Equation (18) in the section on Theoretical Basis (in the Experimental Section). The general expression of r_1^{IS} is given by Equation (6).

$$r_1^{IS} = 1.8 \times 10^{-5}\, q \frac{1}{T_{1M} + \tau_M} \tag{6}$$

Some questionable approximations concerning the electronic relaxation and underlying the SBM relaxation model, which is generally used to interpret the relaxivity data, will be overcome in the present section and further discussed in the section Theoretical Basis (in the Experimental Section). At low field, such approximations lead to an incorrect expression of the theoretical relaxivity involving many unknown parameters. When these parameters are fittted so as this SBM-incorrect expression reproduces the low-field experimental relaxivity, they can take unphysical values to compensate for the drawback of the theory. As recently pointed out by Caravan and co-workers[60] and discussed in the section Theoretical Basis, a proper interpretation of low-field relaxivity data requires a rigorous treatment of the fluctuations of the static zero-field splitting (ZFS). To this end, additional unknown parameters affecting the IS relaxivity have to be introduced, that is, the degree of rhombicity of the static ZFS and the orientation of the Gd^{III}–proton vector $\mathbf{r}_H$ of a coordinated water molecule in the molecular frame of the complex. Then, the theoretical relaxivity r_1 can no longer be expressed in terms of simple analytical expressions as in the SBM approach. It has to be computed either by setting up and inverting the very large matrices of the superoperator Liouville formalism of the general slow-motion theory[19] or by numerical simulation.[20–22] Rather than using the questionable SBM formalism at low field, Troughton et al.[60] contented themselves with interpreting the experimental relaxivity above 0.2 T. Indeed, in this "high"-field region, it depends practically only on the longitudinal electronic relaxation rate $1/T_{1e}$, which is given by general expressions of the McLachlan type.[61–63]

In this paper, we propose a simple three-step method for interpreting the relaxivity profile of the water protons for all field values. The method avoids both the questionable multiparameter fit of the low-field experimental relaxivity by the SBM expression (see the section Theoretical Basis in the Experimental Section) and/or rather complex simulations with additional adjustable parameters. It is based on an independent experimental determination of the electronic relaxation, which makes it self-consistent from an experimental point of view. It consists of measuring the relaxivity of the protons of an auxiliary probe solute that has pure OS intermolecular dynamics with respect to the Gd^{III} complex.

The theoretical OS relaxivity r_1^{OS} is calculated by using the Ayant, Belorizky, Hwang, and Freed (ABHF) analytical formalism.[64–66] The water or diamagnetic solute bearing the observed nuclear spins and the GdL complex are approximated as two hard spheres. These spheres are assumed to carry the nuclear and electronic spins at their centres and to undergo translational Brownian motions in a structureless viscous continuum. Let D_I, D_S be the self-diffusion coefficients of the diamagnetic molecule and GdL complex, respectively. Their relative diffusion coefficient is taken to be $D=D_I+D_S$. Denoting their collision diameter by b, their translational correlation time τ is defined by Equation (7).

$$\tau \equiv b^2/D \tag{7}$$

It is assumed that the quantum motion of the electronic spin S and the OS spatial dynamics of S with respect to the observed nuclear spin I are uncorrelated. Then, the effects of the electronic relaxation on the OS relaxivity r_1^{OS} stem[22,27] from the longitudinal and transverse electronic time correlation functions (TCFs) $G_{\parallel}^{nor}(t)\equiv\langle S_z(t)S_z(0)\rangle/\langle S_z(0)S_z(0)\rangle$ and $G_{\perp}^{nor}(t)\equiv\langle S_+(t)S_-(0)\rangle/\langle S_+(0)S_-(0)\rangle$ of the electron-spin components S_α ($\alpha=x,y,z$). Indeed, r_1^{OS} is a linear combination of spectral densities, which are Fourier–Laplace transforms of the products of the OS intermolecular dipolar TCF $g_2^{OS}(t)$ times $G_{\parallel}^{nor}(t)$ and $G_{\perp}^{nor}(t)$. The decay of $G_{dir}^{nor}(t)$ (dir$=\parallel,\perp$) with time results in values of the product $g_2^{OS}(t)\,G_{dir}^{nor}(t)$, which are smaller than those of $g_2^{OS}(t)$, hence in a relative attenuation of r_1^{OS}. According to recent Monte Carlo simulations,[22,67] the attenuation effect of the longitudinal TCF $G_{\parallel}^{nor}(t)$ is maximum at $B_0=0$ and decreases monotonously with increasing field. The attenuation effect on r_1^{OS} caused by the time decay of the transverse TCF $G_{\perp}^{nor}(t)$ drops similarly as the field increases. However, this decreasing attenuation effect is by far compensated by the stronger and stronger quenching of r_1^{OS} by the faster and faster oscillations of $G_{\perp}^{nor}(t)$ due to the precession of the Gd^{III} spin S at the electronic Larmor frequency ω_S. Our method is based on an effective treatment of the time decays of $G_{\parallel}^{nor}(t)$ and $G_{\perp}^{nor}(t)$, which will be expressed as sums of decreasing exponentials, even if the Redfield–Abragam validity conditions do not hold, so that such expressions are expected to be only approximate.[22,63,67–69]

Let γ_I and γ_S be the gyromagnetic ratios of the proton and electron spins, respectively. In an external field B_0, denote the Larmor angular frequencies of the proton and electron spins by $\omega_I=-\gamma_I B_0$ and $\omega_S=-\gamma_S B_0$. The theoretical form of the OS relaxivity r_1^{OS} depends on the analytical expressions of $G_{\parallel}^{nor}(t)$ and $G_{\perp}^{nor}(t)$. Let D_S^r be the rotational (r) diffusion coefficient of the complex and $\tau_r=\tau_2\equiv 1/(6D_S^r)$ its rotational correlation time. Denote the magnitude of the second-order static ZFS responsible for the low-field electronic relaxation by a_2. The longitudinal electronic TCF $G_{\parallel}^{nor}t)$ was shown to decrease monoexponentially[22,63] at the rate $1/T_{1e}^{analyt}$ given by Equation (8) for $B_0\geq 0.2$ T.

$$\frac{1}{T_{1e}^{analyt}}\equiv\frac{12}{5}a_2^2\tau_r\left(\frac{1}{1+\omega_S^2\tau_r^2}+\frac{4}{1+4\omega_S^2\tau_r^2}\right) \tag{8}$$

As $B_0\rightarrow 0$, the attenuation effect of $G_{\parallel}^{nor}(t)$ on r_1^{OS} is assumed to be still given by an effective monoexponential decay of $G_{\parallel}^{nor}(t)$ at a rate $1/T_{1e}$. Let $1/T_{1e}(B_0=0)\equiv 1/\tau_{S0}^{eff}$ be the effective relaxation rate of this decay at zero field. In the present study, the longitudinal electronic relaxation rate $1/T_{1e}$ is defined by Equation (9).

$$\frac{1}{T_{1e}}=\frac{1}{\tau_{S0}^{eff}}\tanh\left[\left(\frac{1}{T_{1e}^{analyt}}\right)/\left(\frac{1}{\tau_{S0}^{eff}}\right)\right] \tag{9}$$

The physically relevant monotonous decrease of $1/T_{1e}$ versus the proton resonance frequency ν_I [MHz] is shown in Figure 8 for the [Gd(bpatcn)(D_2O)] complex in D_2O with

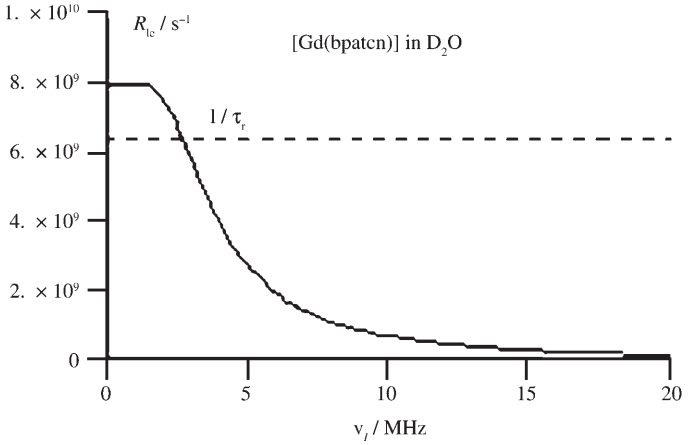

Figure 8. The longitudinal electronic relaxation rate $1/T_{1e}$ of [Gd(bpatcn)(D_2O)] versus the proton resonance frequency ν_I in D_2O at 298 K. The rate $1/T_{1e}$ is defined by Equations (8) and (9). The fluctuating rate of the static ZFS responsible for the low-field electron relaxation is $1/\tau_r$.

the parameters derived hereafter from the application of the method to this complex. As B_0 increases, $1/T_{1e}^{analyt}$ drops rapidly because of its field dispersion in $(\omega_S\tau_r)^{-2}$ and becomes significantly smaller than $1/\tau_{S0}^{eff}$, so that the expected equality $1/T_{1e}\cong 1/T_{1e}^{analyt}$ holds. Moreover, $1/T_{1e}$ smoothly tends to $1/\tau_{S0}^{eff}$ as $B_0\rightarrow 0$. Also note that $1/T_{1e}$ is smaller than or roughly equal to the fluctuating rate $1/\tau_r$ of the static ZFS responsible for the low-field electronic relaxation. This is coherent

with the notion of spin relaxation rate induced by a fluctuating Hamiltonian as discussed by Bertini and co-workers.[69] Now, consider the time decay of the transverse electronic TCF $G_{\perp}^{nor}(t)$. At $B_0=0$, the resonating nuclei are in an isotropic magnetic-field environment, so that $G_{\perp}^{nor}(t)$ decays monoexponentially at the same rate $1/T_{2e,1}(B_0=0)=1/T_{1e}=1/\tau_{S0}^{eff}$ as $G_{\parallel}^{nor}(t)$. For a sufficiently weak static ZFS and a sufficiently short rotational correlation time τ_2, the Redfield–Abragam validity conditions hold.[22,63,70] Then, $G_{\perp}^{nor}(t)$ is a linear combination of four decreasing exponentials $G_{\perp}^{nor}(t)=\exp(i\omega_S t)\ \sum_{i=1}^{4} w_i \exp(-t/T_{2e,i}^{Redfield})$ of weights w_i and rates $1/T_{2e,i}^{Redfield}$, which are obtained by numerical diagonalisation of the Redfield matrix of the transverse electronic relaxation.[70] At $B_0=0$, the weights w_i and rates $T_{2e,i}^{Redfield}$ are such that $w_1=1$, $w_2=w_3=w_4=0$ and $1/T_{2e,i}^{Redfield}(B_0=0)=1/T_{1e}$, so that the expected equality $G_{\perp}^{nor}(t)=G_{\parallel}^{nor}(t)$ is satisfied. In the present study, $G_{\perp}^{nor}(t)$ is still taken to be a weighted sum of four exponentials $G_{\perp}^{nor}(t)=\exp(i\omega_S t)\ \sum_{i=1}^{4} w_i \exp(-t/T_{2e,i})$, where the weights are those of the Redfield theory and the transverse electronic relaxation rates $1/T_{2e,i}$ are defined by Equation (10).

$$\frac{1}{T_{2e,i}}=\frac{1}{\tau_{S0}^{eff}}\tanh\left[\frac{1}{T_{2e,i}^{Redfield}}\Big/\left(\frac{1}{\tau_{S0}^{eff}}\right)\right] \tag{10}$$

Under this approximation, $G_{\perp}^{nor}(t)$ is reasonably accurate within the Redfield limit and the equality $G_{\perp}^{nor}(t)=G_{\parallel}^{nor}(t)$ holds at $(B_0=0)$. Moreover, for the [Gd(bpatcn)(D_2O)] complex in D_2O, the rates $T_{2e,i}$ are smaller than or roughly equal to the fluctuating rate $1/\tau_r$. As B_0 increases, note that $G_{\perp}^{nor}(t)$ affects r_1^{OS} more and more through its fast oscillations due to the precession of the Gd^{III} spin S at the electronic Larmor frequency ω_S, so that a precise description of the time decay of $G_{\perp}^{nor}(t)$ is not necessary.

For both water and probe solute molecules, r_1^{OS} is given by Equation (11) in terms of the ABHF OS spectral density[64,65] $j_{2c}^{OS}(\sigma)$ defined by Equation (12). The argument σ takes the complex values $1/T_{1e}+i\omega_I$ and $1/T_{2e,j}+i\omega_S$ in Equation (11). The function $j_{2c}^{OS}(\sigma)$ is the real part of the Laplace transform of the Hwang and Freed (HF) intermolecular dipolar time correlation function[65,66] (TCF) $g_2^{OS}(t)$ given by Equation (13).

$$r_1^{OS}=\frac{8\pi}{5}\gamma_I^2\gamma_S^2\hbar^2 S(S+1)\left[j_{2c}^{OS}\left(\frac{1}{T_{1e}}+i\omega_I\right)+\frac{7}{3}\sum_{j=1}^{4} w_j j_{2c}^{OS}\left(\frac{1}{T_{2ej}}+i\omega_S\right)\right] \tag{11}$$

$$j_{2c}^{OS}(\sigma)\equiv\frac{10^{-6}N_{Avogadro}}{Db}\,\mathrm{Re}\left[\frac{4+x}{3(9+9x+4x^2+x^3)}\right] \tag{12}$$

with $x\equiv\sqrt{\sigma\tau}$

$$g_2^{OS}(t)\equiv 10^{-6}N_{Avogadro}\frac{18}{\pi b^3}\int_0^{\infty}\exp\left(-\frac{t}{\tau}x^2\right)\frac{x^2\mathrm{d}x}{81+9x^2-2x^4+x^6} \tag{13}$$

The subscript c of j_{2c}^{OS} indicates that the argument of this function is complex. According to Equations (7) to (13), the zero-field theoretical OS relaxivity r_1^{OS} depends on the five parameters D, b, $1/\tau_{S0}^{eff}$, a_2 and τ_r. The relative diffusion coefficient D is taken to be the sum of the experimental values of the self-diffusion coefficient D_I of the probe solute and of the self-diffusion coefficient D_S of LuL, a diamagnetic analogue of GdL that is expected to have the same self-diffusion. Both D_I and D_S were measured[27] with the help of pulsed gradient spin-echo (PGSE) sequences.[71] The collision diameter b of the probe solute and GdL was estimated from compact molecular models. Then, D and b were fixed. The theoretical OS relaxivity r_1^{OS} at zero-field depends only on $1/\tau_{S0}^{eff}$, which was adjusted so as to reproduce the experimental value. Finally, it should be emphasised that the popular interpretation[2,5] of the OS relaxivity of the water protons rests on a questionable application of the ABHF model, for which the minimal distance of approach a_{GdH} between the Gd^{III} nucleus and the proton of a noncoordinated water molecule replaces the collision diameter b. Use of an a_{GdH} distance shorter than b results in an ad hoc increase of the theoretical OS relaxivity. This is necessary to account for many effects, such as the packing of the molecules and the eccentricity of the nuclear spins, which are neglected in the ABHF model and lead to a larger OS relaxivity.

Step one of the method consists in measuring the zero-field relaxivity of the protons of an auxiliary probe solute that has a pure OS intermolecular dynamics with respect to the Gd^{III} complex. The rate $1/\tau_{S0}^{eff}$ is determined as the sole adjustable parameter of the theoretical OS relaxivity r_1^{OS} of the probe solute protons. This avoids having to derive electronic relaxation rates from the questionable SBM expression of $1/T_{1M}$ (see the section Theoretical Basis in the Experimental Section), which in addition has a very rapid variation in r_H^{-6} with the Gd–proton distance r_H allowing one to compensate the defects of the theory by small changes of this distance.

Turning to the practical implementation of step one of the method aimed at determining $1/\tau_{S0}^{eff}$ with the best possible accuracy. According to Equations (11) and (12), the theoretical OS relaxivity $r_1^{OS}(B_0=0)$ at zero field is given by Equation (14).

$$r_1^{OS}(B_0=0)=\frac{16\pi}{3}\gamma_I^2\gamma_S^2\hbar^2 S(S+1)\frac{10^{-6}N_{Avogadro}}{Db}\times\frac{4+x_0}{3(9+9x_0+4x_0^2+x_0^3)} \tag{14}$$

with $x_0\equiv\sqrt{\tau/\tau_{S0}^{eff}}$

For the Gd^{III} complexes in water, x_0 is typically of the order of unity, so that $r_1^{OS}(B_0=0)$ is roughly inversely pro-

portional to b. Any error on this parameter directly affects the zero-field electronic relaxation rate $1/\tau_{S0}^{eff}$, the value of which is adjusted so that the theoretical relaxivity $r_1^{OS}(B_0=0)$ fits its experimental counterpart. To remedy this potential lack of precision, it is preferable to measure the effects of $1/\tau_{S0}^{eff}$ to a relative scale of relaxivity. Consider a reference high (h) field $B_{Oh} \geq 4$–5 T. At B_{Oh}, we have 1) $\omega_I >> 1/T_{1e}$, because the longitudinal electronic relaxation rate $1/T_{1e}$ decreases rapidly with field[22,63] as B_0^{-2}, and 2) $\omega_S >> 1/\tau_{S0}^{eff} \geq 1/T_{2e}$, because $1/\tau_{S0}^{eff}$ is typically[5] of the order of $10^{10}\,s^{-1}$. The values of the spectral densities of Equation (11) can be approximated as $j_{2c}^{OS}(1/T_{1e}+i\omega_I) \cong j_{2c}^{OS}(i\omega_I)$ and $j_{2c}^{OS}(1/T_{2e,i}+i\omega_S) \cong j_{2c}^{OS}(i\omega_S)$. Furthermore, because of the inequalities $\omega_S\tau >> \omega_I\tau$, $\omega_S\tau >> 1$, we have: $j_{2c}^{OS}(i\omega_S) << j_{2c}^{OS}(i\omega_I)$. Then, the theoretical OS relaxivity at B_{Oh} is simply given by Equation (15).

$$r_1^{OS}(B_{Oh}) = \frac{8\pi}{5}\gamma_I^2\gamma_S^2\hbar^2 S(S+1) j_{2c}^{OS}(i\omega_I(B_{Oh})) \qquad (15)$$

The relative scale of relaxivity is introduced through the relaxivity ratio q_1^{OS} defined by Equation (16).

$$q_1^{OS} \equiv \frac{3}{10}\frac{r_1^{OS}(B_0=0)}{r_1^{OS}(B_{Oh})} \qquad (16)$$

Setting $x_0 \equiv \sqrt{\tau/\tau_{S0}^{eff}}$ and $x_h \equiv \sqrt{i\omega_I(B_{Oh})\tau}$, q_1^{OS} simplifies to Equation (17) according to Equations (11), (12), and (15).

$$q_1^{OS} = \left[\frac{4+x_0}{9+9x_0+4x_0^2+x_0^3}\right] / \mathrm{Re}\left[\frac{4+x_h}{9+9x_h+4x_h^2+x_h^3}\right] \qquad (17)$$

The value of $1/\tau_{S0}^{eff}$ is adjusted so that the theoretical relaxivity ratio q_1^{OS} fits its experimental counterpart.

In step two, the ABHF model of the OS dynamics of GdL with respect to the probe solute is tested together with the electronic relaxation model defined by the relaxation rates $1/T_{1e}$ and $1/T_{2e,i}$ given by Equations (8)–(10). The rotational correlation time τ_2 is estimated from the volume of GdL by using a Stokes-Einstein-like equation to describe the rotational diffusion. The test is to compare the theoretical OS relaxivity r_1^{OS} of the probe solute protons given by Equations (7) to (13) with its experimental counterpart over a large field range.

Step three is to check whether the experimental water proton relaxivity r_1 is satisfactorily represented by the usual Equations (5), (6), (18), (19), and (7)–(13), but with the relaxation rates $1/T_{1e}$ and $1/T_{2e,i}$ given by Equations (8)–(10).

NMRD interpretation: We have applied the above theoretical framework for the interpretation of the relaxivity profiles of [Gd(bpatcn)(H_2O)]. The neutral *tert*-butyl alcohol $(CH_3)_3COD$ molecule was chosen as probe solute for the following three reasons: 1) It has a nearly spherical shape. 2) It carries nine equivalent protons giving rise to a large NMR signal on the FFC relaxometer, even at the used semi-dilute concentration $\cong 0.4$ M. This allows one to keep the concentration of the probe solute low enough for not perturbing the microdynamics of [Gd(bpatcn)(H_2O)] significantly. 3) It is expected not to undergo any association with the Gd^{III} complex, so that the proton relaxation mechanism due to this paramagnetic ion is purely OS. The relaxivity profile of the $(CH_3)_3COD$ protons in a solution of [Gd(bpatcn)(D_2O)] in D_2O at 298 K is shown in Figure 9.

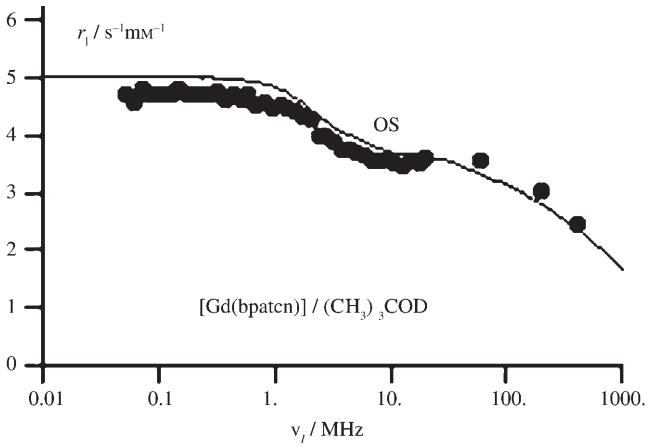

Figure 9. Longitudinal relaxivity r_1 of the protons on the $(CH_3)_3COD$ probe solute in a solution of [Gd(bpatcn))(D_2O)] in deuterated water at 298 K.

The measured self-diffusion coefficients of $(CH_3)_3COD$ and [Gd(bpatcn)(D_2O)] are $D_I = 0.57\times10^{-5}\,cm^2s^{-1}$ and $D_S = 0.37\times10^{-5}\,cm^2s^{-1}$, respectively. The collision diameter of these species is estimated to be $b = 6.5$ Å to within 10%.

Turn to step one of the method. To determine $1/\tau_{S0}^{eff}$ from Equation (17), a reference high-field B_{Oh} is needed. If its value is chosen to be $B_{Oh} = 9.4$ T ($\nu_I = 400$ MHz), we get $1/\tau_{S0}^{eff} = 0.8\times10^{10}\,s^{-1}$. Now, change the value of b by 10%. The estimate of $1/\tau_{S0}^{eff}$ derived from the relaxivity ratio q_1^{OS} varies by only about 5%. Furthermore, the value of $1/\tau_{S0}^{eff}$ derived from q_1^{OS} should be independent of the choice of B_{Oh} to within the experimental accuracy. This can be checked in the case of $B_{Oh} = 4.7$ T ($\nu_I = 200$ MHz), for which we get the estimate $1/\tau_{S0}^{eff} = 0.76\times10^{10}\,s^{-1}$, which is equal to the value derived at 400 MHz to within 5%.

In step two of the method, the theoretical OS relaxivity r_1^{OS} of the $(CH_3)_3COD$ protons is calculated by Equations (11) and (12), and compared to the experimental data over the whole frequency range. Using molecular models, the minimal distance of approach between the Gd^{III} nucleus and the protons of the probe solute is estimated to be $a_{GdH}((CH_3)_3COD) \cong 4.7$ Å. The electronic relaxation rates $1/T_{1e}$ and $1/T_{2e,i}$ are given by Equations (8)–(10), in which the magnitude of the second-order static ZFS is $a_2 = 0.65\times10^{10}\,rad\,s^{-1}$ and the rotational correlation time of [Gd(bpatcn)(D_2O)] in D_2O is $\tau_r = 158$ ps. The value of a_2 is typical[21,70] for polyaminocarboxylate complexes of Gd^{III} and is chosen so as to produce the observed decrease of the experimental relaxivity between 1 and 10 MHz. The value

of τ_r was obtained as follows. Consider a sphere $S_{Gd(bpatcn)}$ having the same volume as the ellipsoid that best approximates [Gd(bpatcn)(D_2O)]. Let $S_{Gd(dtpa)}$ be the analogous sphere for [Gd(dtpa)(H_2O)], the rotational correlation time of which was estimated to be $\tau_{r,Gd(dtpa)} \cong 65.8$ ps in H_2O at 298 K by a careful EPR study at various temperatures and fields.[70] Let d_1, d_2, d_3 be the lengths of the principal axes of the ellipsoids approximating the complexes as defined by compact molecular models. The radius of the sphere having the same volume is simply $a_{complex} = 0.5\sqrt{d_1 d_2 d_3}$. We measured $a_{Gd(bpatcn)} \cong 4.8$ Å and $a_{Gd(dtpa)} \cong 4.0$ Å. The rotational diffusion coefficients $D^r_{S,Gd(bpatcn)\text{ in }D_2O}$ and $D^r_{S,Gd(dtpa)\text{ in }H_2O}$ of the complexes were assumed to obey the Stokes–Einstein-like law, which incorporates a microviscosity factor and was used previously.[70] The rotational correlation time τ_r of [Gd(bpatcn)(D_2O)] was calculated as $\tau_r = (D^r_{S,Gd(dtpa)\text{ in }H_2O} / D^r_{S,Gd(bpatcn)\text{ in }D_2O})\tau_{r,Gd(dtpa)}$ by using the radii of the spheres approximating the complexes and the ratio $\eta(D_2O)/\eta(H_2O) = 1.24$ of the viscosities[72] of D_2O and H_2O. As shown in Figure 9, the theoretical profile is in good agreement with the experimental one.

Step three of the method deals with the relaxivity of the H_2O protons. Since the complex [Gd(bpatcn)(H_2O)] in H_2O and its deuterated analogue [Gd(bpatcn)(D_2O)] in D_2O have the same volume, their rotational correlation times are proportional to the viscosities of the solvents with the same proportionality constant according to the Stokes–Einstein equation. The ratio of the viscosities[72] of D_2O and H_2O is $\eta(D_2O)/\eta(H_2O) = 1.24$, so that the rotational correlation time τ_2 used in this section for calculating the relaxation rates $1/T_{1e}$ and $1/T_{2e,i}$ by Equations (8)–(10) was $\tau_r = \tau_r(H_2O) = \tau_r(D_2O)/1.24 = 127$ ps. To calculate the IS relaxivity, we used the following IS parameters: The number $q = 1$ of metal-bound water molecules introduced in Equation (6) was derived from independent luminescence decay studies. The Gd–proton distance $r_H = 3.23$ Å used to calculate $1/T_{1M}$ according to Equations (18) and (19) was taken to be in the range of the values[5,73] generally obtained for the Gd^{III} complexes and compatible with the known X-rays crystal structures. The lifetime τ_M was determined so as to be compatible with general features of the experimental longitudinal and transverse relaxivities r_1 and r_2 of the water protons. Let $\Delta r_1 = r_1(0) - r_1(B_{Oh})$ be the difference between the values of r_1 at zero field and a high field B_{Oh} corresponding to one of the resonance frequencies $\nu_{lh} = 200$, 400 or 500 MHz. The differences between the theoretical and experimental values of Δr_1 and r_2 become notable for $\tau_M \geq 4$ μs and increase with τ_M. For instance, if $\tau_M = 4$ μs, the theoretical values of Δr_1 and r_2 are typically about 80% and 93% of their experimental counterparts, when the other molecular parameters keep reasonable values. The growing influence of τ_M, as it becomes longer and longer, and the possibility to discriminate between τ_M values result from the Equation (6) of r_1^{IS} and from a similar equation giving r_2^{IS}. Indeed, as soon as τ_M has a significant duration with respect to T_{1M} and T_{2M}, the dispersion of T_{1M} with field and the difference between T_{1M} and T_{2M} at high field lead to variations of r_1 and r_2, showing a dependence on τ_M, which is large enough to discriminate between possible estimates of this lifetime. From the above considerations, τ_M has to be significantly smaller than 4 μs. Besides, for $\tau_M \leq 1$ μs, the theoretical values of Δr_1 and r_2 are typically larger than their experimental counterparts by about 20 and 10%, or more, when the other molecular parameters keep reasonable values. Therefore, the lifetime was estimated to be the geometrical mean of the bounds 1 μs and 4 μs of the interval of its reasonable values, that is, $\tau_M = 2$ μs, which is in the range of known values for this type of complexes.[2,5] The precise value retained for τ_M in the middle of the range [1, 4 μs] modestly affects the theoretical relaxivities and is not relevant for the interpretation of their experimental counterparts. However, note that the value $\tau_M = 1.7$ μs was obtained from an independent ^{17}O NMR study.[74] It should be emphasised that the water-exchange lifetime could be reasonably estimated from the present relaxivity data, because of the additional information provided by the probe solute and the high-field T_1 and T_2 measurements. Additional OS parameters are needed to calculate the OS relaxivity. As for the probe solute, the theoretical OS relaxivity r_1^{OS} of the water protons depends on D, a_{GdH}, $1/T_{1e}$, and $1/T_{2e,j}$. Again, the relative diffusion coefficient D was taken to be the sum of the self-diffusion coefficients D_I of water and D_S of [Gd(bpatcn)(H_2O)]. The self-diffusion coefficient of H_2O in light water was assumed to have its usual measured value $D_I = 2.3 \times 10^{-5}$ cm^2 s^{-1}. The self-diffusion coefficient D_S of [Gd(bpatcn)(H_2O)] in H_2O was calculated from the measured value of its deuterated analogue [Gd(bpatcn)(D_2O)] in D_2O by assuming that it is simply inversely proportional to the solvent viscosity, according to the Stokes–Einstein law for the translational Brownian motion. Thus, $D_S(\text{in } H_2O) = 1.24 D_S$ (in D_2O) $= 0.46 \times 10^{-5}$ cm^2 s^{-1} and $D = 2.75 \times 10^{-5}$ cm^2 s^{-1}. By using compact molecular models, the minimal distance of approach between the Gd^{III} nucleus and the protons of a non-coordinated water molecule was estimated to be $a_{GdH} \cong 4.3$ Å. As shown in Figure 10, the theoretical relaxivity profile of the H_2O protons is in good agreement with the experimental

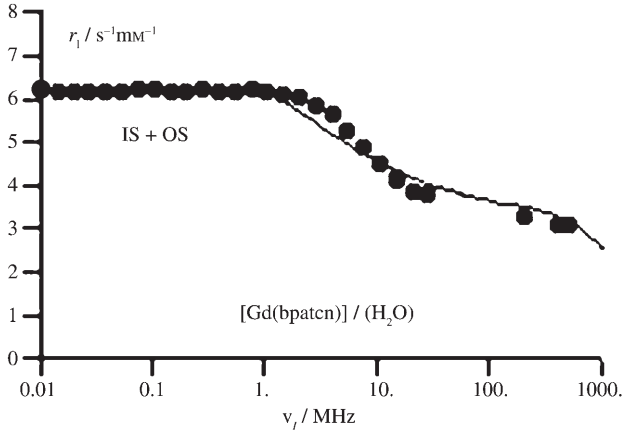

Figure 10. Longitudinal relaxivity r_1 of the H_2O protons in a solution of [Gd(bpatcn))(H_2O)] in water at 298 K.

one. Furthermore, the theoretical values 4.19, 4.09 4.03 s^{-1} mM^{-1} of r_2 at 200, 400 and 500 MHz compare favourably with their experimental counterparts 4.04, 3.99 and 4.03 s^{-1} mM^{-1}.

To compare the new theoretical method presented in this work with the traditional SBM approach, the longitudinal relaxivity r_1 of the H_2O protons in a solution of [Gd(bpatcn))(H_2O)] in water at 298 K was also interpreted within the framework of the popular SBM theory,[2,5] sketched in the Theoretical Basis section (in the Experimental Section). The theoretical curve shown in Figure S4 (in the Supporting Information) was calculated with the parameters reported in the caption and had typical values for a polyaminocarboxylate complex.[5] It reproduced the experimental data quite satisfactorily. Then, it was tempting to test whether the SBM description of the electronic relaxation of the Gd^{III} spin S, successfully used to intepret the H_2O relaxivity, could also provide a theoretical relaxivity profile of the $(CH_3)_3$COD protons in good agreement with its experimental counterpart of a solution of [Gd(bpatcn))(D_2O)] in deuterated water at 298 K. For that purpose, we calculated the McLachlan-type electronic relaxation rates $1/T_{1e}$ and $1/T_{2e}$ involved in the SBM theory and defined by Equations (21)–(23) with the electronic relaxation parameters $\tau_{S0}(H_2O) = 130$ ps and $\tau_v^{ad\,hoc} = 25$ ps derived from the interpretation of the H_2O profile. Substituting $1/T_{1e}$ and $1/T_{2e}$ for these particular values in the ABHF OS spectral densities occuring in the general expression of r_1^{OS} as discussed in the Theoretical Basis section (in the Experimental Section), we obtained the ABHF OS relaxivity formula of the $(CH_3)_3$COD protons. Since the relative diffusion coefficient D has the experimental value given in the NMRD Interpretation section, the only adjustable parameter of the ABHF OS formula remains the minimal distance of approach $a_{GdH}((CH_3)_3COD)$ between Gd^{III} and the $(CH_3)_3$COD protons. The theoretical SBM relaxivity profile of the $(CH_3)_3$COD protons was fitted to the experimental values as shown in Figure 11. To reproduce the high-frequency data, the minimal distance of approach was taken to be $a_{GdH}((CH_3)_3COD) = 4.55$ Å. Unfortunately, this value is too small for the rather bulky $(CH_3)_3$COD molecule. Furthermore, the electronic relaxation model successfully used for interpreting the water proton relaxivity leads to a relaxivity profile of the $(CH_3)_3$COD protons, displaying low-frequency values, which are too high, and then an unphysical sharp decrease in the range of the proton frequency ν_I between 1 and 10 MHz. This is a typical example of contradiction raised by the popular SBM approach, which does not properly account for the physical processes underlying the electronic relaxation.

The relaxivity profile of [Gd(bpatcn))(H_2O)] is very similar to that observed for the monoaqua commercial contrast agent [Gd(dtpa)(H_2O)]$^{2-}$. However, the measured electron spin relaxation time at zero field is longer for [Gd(bpatcn))(H_2O)] ($\tau_{S0}^{eff} = 125$ ps) with respect to the dtpa complex ($\tau_{S0}^{eff} = 72$ ps). Due to the important influence of the coordination environment on the electronic relaxation, very disparate values are found for the electronic relaxation time

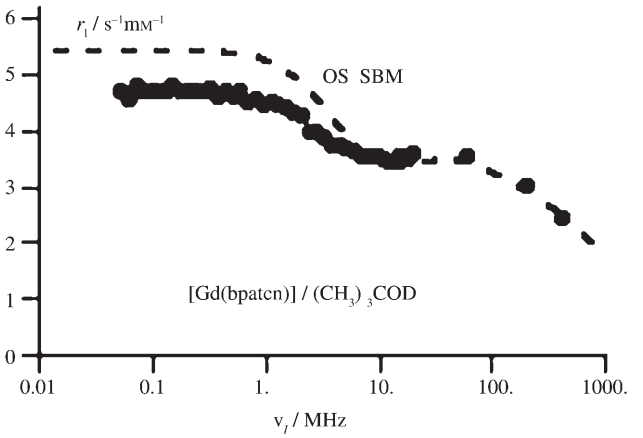

Figure 11. Alternative interpretation of the longitudinal relaxivity r_1 of the protons on the $(CH_3)_3$COD probe solute in a solution of [Gd(bpatcn))(D_2O)] in deuterated water at 298 K within the framework of the popular SBM theory[2,5] sketched in the Theoretical Basis section (in the Experimental Section). The relative diffusion coefficient D has the experimental value given in the NMRD Interpretation section. The parameters of the McLachlan-type electronic relaxation rates adjusted to reproduce the water proton relaxivity of Figure S3 (see Supporting Information) are $\tau_{S0}(H_2O) = 130$ ps and $\tau_v^{ad\,hoc} = 25$ ps. The adjusted minimal distance of approach between Gd^{III} and the $(CH_3)_3$COD protons is $a_{GdH}((CH_3)_3COD) = 4.55$ Å.

at zero field in gadolinium complexes.[5,35] Although it is generally accepted that a highly symmetric coordination sphere can lead to slow low-field electronic relaxation, other molecular parameters such as the type of donor atoms[29] or the complex rigidity can influence the electronic relaxation of gadolinium complexes and make its optimisation difficult. The value of the electron-spin relaxation time at zero field found for the gadolinium complex of the asymmetric ligand bpatcn^{3-} ($\tau_{S0}^{eff} = 125$ ps) is similar to the value reported for the Gd^{III} complex of the C_3 symmetric ligand nota^{3-} ($\tau_{S0}^{eff} = 131$ ps).[35] In spite of the similar molecular symmetry, the complex [Gd(tpatcn)] shows a much longer value of τ_{S0}^{eff} (1500 ps) with respect to [Gd(nota)(H_2O)$_3$]. This value, which is the longest reported to date for a gadolinium complex, was attributed to the presence of an unusually high number of N-donor atoms. The replacement of one picolinate arm in the symmetric ligand H_3tpatcn with one acetate arm leads to a drastic shortening of the electron relaxation time at zero field probably due to the decreased symmetry. However, the electron relaxation rate of [Gd(bpatcn)(H_2O)] at zero field is significantly slower than that observed for the [Gd(bpeda)(H_2O)]$^-$, which also presents an asymmetric arrangement of the picolinate arms. The difference between these two very similar nine-coordinate gadolinium complexes can be interpreted in terms of a residual local symmetry provided by the triazacyclononane macrocycle in the bpatcn^{3-}. However, the increased structural rigidity and the higher number of N-donor atoms could also have a significant influence and additional studies on related systems are in progress to investigate further the influence of the molecular structure on the electronic relaxation.

Conclusion

The introduction of two picolinate groups and one carboxylate on the triazacyclononane core produces the ligand H_3bpatcn, which binds to lanthanide ions in a octadentate fashion. The presence of two additional pyridine nitrogen atoms leads to an increased stability of the Gd^{III} complexes of H_3bpatcn with respect to those of the analogous ligand H_3nota and improves the selectivity for Gd^{III} over Ca^{II}. The results reported here show that the pyridyl group, when appropriately introduced in the ligand design, is efficient in providing increased selectivity and stability of lanthanide complexes for biomedical applications. The ligand architecture has proved to be well adapted to lanthanide ion complexation, in spite of its asymmetric structure. Accordingly the complexes of $bpatcn^{3-}$ adopt a C_1 symmetric structure in solution in which the macrocyclic framework and the pendant arms remain bound and rigid (for the smaller lanthanide ions) on the NMR timescale, affording enantiomeric pairs. Despite the presence of a coordinated water molecule the molecular architecture of $bpatcn^{3-}$ sensitise Eu^{III} and Tb^{III} luminescence efficiently and yields a terbium complex with long luminescence lifetime and high luminescence quantum yield. The intense luminescence associated to the water solubility and physiological stability indicate that the complex $[Tb(bpatcn)(H_2O)]$ is well adapted for the development of luminescent labels for biomedical applications such as time-resolved fluoroimmunoassays.

The nine-coordinate gadolinium–$bpatcn^{3-}$ complex displays a relaxivity at imaging fields similar to that reported for the commercial contrast agents $[Gd(dota)(H_2O)]^-$ and $[Gd(dtpa)(H_2O)]^{2-}$ and to the relaxivity observed for the analogous nine-coordinate complex $[Gd(bpdea)(H_2O)]^-$. A new theoretical framework was proposed for the interpretation of the relaxivity profile of the H_2O protons. It is based on an independent experimental determination of the zero-field electronic relaxation rate by using a neutral probe solute that has purely outer-sphere (OS) intermolecular dynamics with respect to the complex. It replaces the Solomon, Bloembergen and Morgan (SBM) framework, which is questionable at low field as evidenced by the poor agreement between the experimental relaxivity profile of the $(CH_3)_3COD$ protons and its theoretical counterpart provided by the SBM description of the electronic relaxation. It avoids resorting to simulations and/or sophisticated theories with additional unknown zero-field splitting (ZFS) parameters.

Moreover, the access to a model-independent experimental determination of the zero-field electronic relaxation rate should help to elucidate the influence of the molecular structure on the electronic relaxation opening an entry into the molecular programming of the electronic relaxation. The comparison of the electronic relaxation rates observed in picolinate complexes shows that in spite of the presence of similar donor atoms, and of the asymmetric coordination polyhedron of both complexes, the electron-spin relaxation time at zero field of the $[Gd(bpatcn)(H_2O)]$ complex is significantly longer than in the analogous complex $[Gd(bpeda)(H_2O)]^-$. The replacement of one picolinate arm in the symmetric ligand H_3tpatcn with an acetate arm results in an important shortening of the zero-field electronic relaxation time of the $[Gd(bpatcn)(H_2O)]$ complex with respect to the analogous $[Gd(tpatcn)]$ complex; however, the inclusion of picolinate groups on a triazacyclononane framework to afford a monoaquo gadolinium complex leads to a more favourable electron relaxation than that of the complex $[Gd(bpeda)(H_2O)]^-$. In addition preliminary multifield EPR experiments indicate an electronic relaxation at 1.2 T slower than $[Gd(dota)(H_2O)]^-$, the electron-spin relaxation of which is unlikely to limit the attainable relaxivity when included in macromolecular systems. These results show the importance of an appropriate ligand design in the optimisation of the electronic relaxation rate. Moreover the facile functionalisation of $bpatcn^{3-}$ for the access to macromolecular contrast agents with longer correlation times should allow to study the influence of the optimisation of the electronic relaxation on the relaxivity of high molecular weight systems.

Experimental Section

General information: Solvents and starting materials were obtained from Aldrich, Fluka, Acros and Alfa and used without further purification. 6-Chloromethylpyridine-2-carboxylic acid ethyl ester was obtained from the commercially available 2,6-dipicolinic acid according to a published procedure.[75]

Synthesis of the ligand H_3bpatcn

1,4-Bis[(6-carbethoxypyridin-2-yl)methyl]-1,4,7-triazacyclononane (1): 1,4,7-Triazacyclononane trihydrochloride (0.431 g, 1.81 mmol) and K_2CO_3 (1.05 g, 7.62 mmol) were successively added to a solution of 6-chloromethylpyridine-2-carboxylic acid ethyl ester (0.760 g, 3.81 mmol) in anhydrous acetonitrile (50 mL) under argon atmosphere. After stirring at room temperature for one hour, the reaction mixture was refluxed for 18 h. After removal of the inorganic salts by filtration and evaporation of the solvent, the resulting crude product was purified by column chromatography on alumina activity III (50 g, CH_2Cl_2/EtOH 100 to 98/2) to give **1** as a yellow oil (0.193 g, 24%). ^{1}H NMR (400 MHz, CD_3CN, 298 K): $\delta =$ 1.35 (t, $J = 7.0$ Hz, 6H; $COOCH_2CH_3$), 2.70 (s, 4H; $N(CH_2)_2N$), 2.83 (t, $J = 5.2$ Hz, 4H; $N(CH_2)_2N$), 2.92 (t, $J = 5.2$ Hz, 4H; $N(CH_2)_2N$), 3.92 (s, 4H; NCH_2py), 4.38 (q, $J = 7.0$ Hz, 4H; $COOCH_2CH_3$), 7.60 (d, $J =$ 7.6 Hz, 2H; *CH*), 7.75 (t, $J = 7.6$ Hz, 2H; *CH*), 7.92 ppm (d, $J = 7.6$ Hz, 2H; CH); ^{13}C NMR (100 MHz, CD_3CN, 298 K): $\delta = 14.51$ (primary C), 47.26, 52.15, 53.54, 62.37, 62.84 (secondary C), 124.20, 127.29, 138.46 (tertiary C), 148.43, 161.71, 166.14 ppm (quaternary C); ES-MS: *m/z*: 456.3 $[M+H]^+$.

1-Carbethoxymethyl-4,7-bis[(6-carbethoxypyridin-2-yl)methyl]-1,4,7-triazacyclononane (2): Ethyl chloroacetate (0.255 g, 2.08 mmol) and K_2CO_3 (0.288 g, 2.08 mmol) were successively added to a solution of **1** (0.860 g, 1.89 mmol) in anhydrous acetonitrile (60 mL). The reaction mixture was refluxed overnight. After filtration and evaporation of the solvent, the resulting crude product was purified by column chromatography on alumina activity III (90 g, CH_2Cl_2/EtOH 100 to 98/2) to produce **2** as a yellow oil (0.568 g, 56%). ^{1}H NMR (400 MHz,$CDCl_3$, 298 K): $\delta = 1.29$ (t, $J =$ 6.8 Hz, 3H; $COOCH_2CH_3$), 1.46 (t, $J = 7.2$ Hz, 6H; $pyCOOCH_2CH_3$), 2.91 (s, 4H; $N(CH_2)_2N$), 2.95 (s, 8H; $N(CH_2)_2N$), 3.44 (s, 2H; CH_2COOEt), 4.01 (s, 4H; NCH_2py), 4.18 (q, $J = 6.8$ Hz, 2H; $COOCH_2CH_3$), 4.50 (q, $J = 7.2$ Hz, 4H; $pyCOOCH_2CH_3$), 7.83 (m, 4H; CH), 8.01 ppm (t, $J = 4.8$ Hz, 2H; CH); ^{13}C NMR (100 MHz, CD_3CN, 298 K): $\delta = 14.54$, 14.60 (primary C), 55.29, 56.30, 60.82, 62.25 (secondary

C), 124.11, 127.38, 138.34 (tertiary C), 148.50, 166.19, 172.80 ppm (quaternary C). ES-MS: *m/z* (%): 542.3 (100) $[M+H]^+$, 564.3 (20) $[M+Na]^+$.

1-Carboxymethyl-4,7-bis[(6-carboxypyridin-2-yl)methyl]-1,4,7-triazacyclononane (H_3bpatcn): A 1 M aqueous solution of potassium hydroxide (6.5 mL) was added to a solution of **2** (0.321 g, 0.570 mmol) in ethanol (10 mL). The reaction mixture was refluxed overnight. After evaporation of the solvent, the resulting oil was dissolved in water and the pH was adjusted to 1.5 by adding a 1.2 M hydrochloric acid solution in water. Slow evaporation of this solution produced the ligand H_3bpatcn·2.5 KCl·2 HCl·4 H_2O as white crystals (0.310 g, 69 %). ^{1}H NMR (400 MHz, D_2O, 298 K, pD 6.4): δ = 3.53 (s, 8H; N(CH_2)$_2$N), 3.58 (s, 4H; N(CH_2)$_2$N), 3.83 (s, 2H; CH_2COOH), 4.50 (s, 4H; NCH_2py), 7.58 (d, J = 7.6 Hz, 2H; *CH*), 7.86 (d, J = 7.6 Hz, 2H; CH), 7.96 ppm (t, J = 7.6 Hz, 2H; CH); ^{13}C NMR (100 MHz, D_2O, 298 K): δ = 50.55, 50.98, 51.08, 57.97, 59.03 (secondary C), 125.18, 127.36, 140.66 (tertiary C), 146.42, 153.50, 166.87, 170.51 ppm (quaternary C); ES-MS : *m/z* (%): 458.2 (100) $[M+H]^+$, 496.2 (20) $[M+K]^+$; elemental analysis calcd (%) for $C_{22}H_{27}N_5O_6$·2.5 KCl·2 HCl·4 H_2O (788.85): C 33.49, H 4.73, N 8.88; found: C 33.49 H 4.72 N 8.77; the salt content was confirmed by potentiometric titration.

Synthesis of the lanthanide complexes

[Eu(bpatcn)]: A solution of $EuCl_3$·6 H_2O (0.13 mmol) in water (0.4 mL) was added to a solution of H_3bpatcn (0.15 mmol) in water (2 mL). The pH of the resulting mixture was adjusted (pH 7.5) by adding an aqueous KOH solution (1 M). After evaporation of the water the resulting solid was suspended in ethanol (20 mL). The resulting suspension was refrigerated at 4 °C overnight and the solid (KCl) was removed by filtration. Slow evaporation of the resulting solution yielded the [Eu(bpatcn)] complex as a white microcrystalline solid (66.3 mg, 65 %). ES-MS: *m/z* (%): 646.0 (100) [Eu(bpatcn)+K]$^+$, 949.1 (78) [3 Eu(bpatcn)+2 K]$^{2+}$, 1251.0 (75) [2 Eu(bpatcn)+K]$^+$; elemental analysis calcd (%) for [Eu(bpatcn)]·4.5 H_2O·1.3 KCl (784.41): C 33.69, H 4.24, N 8.93; found: C33.54/33.72, H 4.25/4.36, N 8.86.

[La(bpatcn)] and [Lu(bpatcn)]: The complexes [La(bpatcn)] and [Lu(bpatcn)] were isolated following the same procedure. ES-MS [La(bpatcn)]: *m/z* (%): 594.2 (100) [2 La(bpatcn)+2 H]$^{2+}$, 891.1 (28) [3 La(bpatcn)$_3$+2 H]$^{2+}$, 1187.2 (55) [2 La(bpatcn)+H]$^+$; ES-MS [Lu(bpatcn)]: *m/z* (%): 668.2 (100) [Lu(bpatcn)+K]$^+$, 982.9 (18) [3 Lu(bpatcn)+2 K]$^{2+}$, 1297(18) [2 Eu(bpatcn)+K]$^+$.

Solution NMR studies: ^{1}H and ^{13}C NMR spectra were recorded on a Varian Unity 400 spectrometer. Chemical shifts are reported in ppm with solvent as internal reference. The chemical shift of HDO was adjusted as a function of the temperature by using the equation of Nudelman.[76] The samples of the Ln^{III} (Ln = Lu, La) complexes for the NMR measurements were prepared by dissolving equimolar amounts of the ligand and of the hydrate $LnCl_3$ in D_2O followed by adjustement of the pD with solutions of NaOD in D_2O. The Eu^{III} samples were prepared by dissolving the appropriate amount of [Eu(bpatcn)]·4.5 H_2O·1.3 KCl in D_2O. Concentrations in the range of 2×10^{-2}–4×10^{-2} M were used. The pH values given are corrected for D isotope effects.[77] The proton resonances were assigned by 2D COSY and NOESY experiments. In the EXSY spectra a 600 ms mixing times was found to give good intensity of cross-peaks.

[La(bpatcn)]: ^{1}H NMR (400 MHz, D_2O, 298 K, pD = 7.1): δ = 2.40 (br, 2H; CH_2(tcn)), 2.82 (br, 2H; CH_2(tcn)), 3.02 (br,8H; CH_2(tcn)), 3.35(s, 2H; H_7), 4.18 (br, 2H; H_{8a}/H_{8b}), 4.68 (d, J = 14.8 Hz, 2H H_{8a}/H_{8b}), 7.74 (d, J = 7.6 Hz, 2H; H_9), 8.07 (d, J = 7.6 Hz, 2H; H_{11}), 8.17 ppm (t, J = 7.6 Hz, 2H; H_{10}).

[Lu(bpatcn)]: ^{1}H NMR (400 MHz, D_2O, 298 K, pD = 4.2): δ = 2.02 (td, ^1J = 13.3 Hz, ^2J = 5.6 Hz, 1H; CH_2(tcn)), 2.21 (td, ^1J = 12.9 Hz, ^2J = 5.6 Hz, 1H; CH_2(tcn)), 2.50 (dd, ^1J = 12.9 Hz, ^2J = 5.1 Hz, 1H; CH_2(tcn)), 2.63 (dd, ^1J = 12.9 Hz, ^2J = 5.1 Hz, 1H; CH_2(tcn)), 2.77–2.84 (m, 3H; CH_2(tcn)), 2.92 (dd, ^1J = 16.0 Hz, ^2J = 5.5 Hz, 1H; CH_2(tcn)), 3.33, 3.41 (AB system, J_{AB} = 16.0 Hz, 1H; H_7/$H_{7'}$), 3.44–3.59 (m, 4H; CH_2(tcn)), 4.04, 4.15 (AB system, J_{AB} = 14.8 Hz, 2H; H_{8a}/$H_{8b'}$), 4.27, 4.46 (AB system, J_{AB} = 14.8 Hz, 2H; H_{8a}/H_{8b}), 7.72 (d, J = 7.4 Hz, 1H; $H_{9'}$), 7.81 (d, J = 7.4 Hz, 1H; H_9), 8.03 (d, J = 7.8 Hz, 1H; H_{11}), 8.08 (d, J = 7.8 Hz, 1H; $H_{11'}$), 8.19 (t, J = 7.4 Hz, 1H; $H_{10'}$), 8.21 ppm (t, J = 7.8 Hz, 1H; H_{10}).^{1}H NMR (400 MHz, D_2O, 343 K, pD = 4.2): δ = 1.98 (td, ^1J = 13.2 Hz, ^2J = 5.6 Hz, 1H; CH_2(tcn)), 2.17 (td, ^1J = 13.4 Hz, ^2J = 5.6 Hz, 1H; CH_2(tcn)), 2.48 (dd, ^1J = 12.4 Hz, ^2J = 4.8 Hz, 1H; CH_2(tcn)), 2.62 (dd, ^1J = 12.4 Hz, ^2J = 4.8 Hz, 1H; CH_2(tcn)), 2.80 (m, 3H; CH_2(tcn)), 2.88 (dd, ^1J = 16.4 Hz, ^2J = 5.6 Hz, 1H; CH_2(tcn)), 3.79, 3.86 (AB system, J_{AB} = 27 Hz, 2H; H_7/$H_{7'}$), 3.45–3.56 (m, 4H; CH_2(tcn)), 4.48, 4.58 (AB system, J_{AB} = 14.6 Hz , 2H; $H_{8a'}$/$H_{8b'}$), 4.70, 4.90 (AB system, J_{AB} = 15.0 Hz, 2H; H_{8a}/H_{8b}), 7.71 (d, J = 7.2 Hz, 1H; $H_{9'}$), 7.8 (d, J = 7.6 Hz, 1H; H_9), 8.03 (d, J = 7.6 Hz, 1H; H_{11}), 8.09 (d, J = 7.2 Hz, 1H; $H_{11'}$), 8.19 (t, J = 7.2 Hz, 1H; $H_{10'}$), 8.21 ppm (t, J = 7.6 Hz, 1H; H_{10}).

[Eu(bpatcn)]: ^{1}H NMR (400 MHz, D_2O, 400 MHz, 343 K, pD = 9.1): δ = −11.97 (s, 1H; H_1/H_2), −10.26 (s, 1H; H_3/H_4), −7.26 (s,1H; H_5/H_6), −4.79 (s, 1H; H_3/H_4), −3.30 (s,1H; H_1/H_2), −3.16 (s, 1H; H_5/H_6), −0.84 (s, 1H; $H_{8a'}$/$H_{8b'}$), 0.45 (s, 1H; $H_{1'}$/$H_{2'}$), 0.52 (s, 1H; H_5/$H_{6'}$), 0.52 (s, 1H; H_7/$H_{7'}$), 0.86 (s, 1H; H_5/$H_{6'}$), 2.26 (s, 1H; $H_{3'}$/$H_{4'}$), 2.46 (s, 1H; H_3/$H_{4'}$), 4.22 (s, 1H; H_7/$H_{7'}$), 4.35 (s, 1H; H_{8a}/H_{8b}), 5.19 (d, J = 7.2 Hz,1H; H_{11}), 6.34 (d, J = 7.2 Hz, 1H; H_9), 7.29 (t, J = 7.6 Hz, 1H; H_{10}), 7.41 (d, J = 6.8 Hz, 1H; $H_{11'}$), 7.57 (s, 1H; H_{8a}/H_{8b}), 8.40 (d, J = 7.2 Hz, 1H; $H_{9'}$), 9.68 (t, J_1 = 7.2 Hz, J_2 = 7.6 Hz, 1H; $H_{10'}$), 11.07 (s, 1H; H_{8a}/$H_{8b'}$), 16.75 ppm (s, 1H; $H_{1'}$/$H_{2'}$); ^{1}H NMR (400 MHz, D_2O, 278 K, pD = 9.1): δ = −15.61 (br, 1H; H_1/H_2), −13.83 (br, 1H; H_3/H_4), −9.65 (s,1H; H_5/H_6), −7.73 (br, 1H; H_3/H_4), −5.82 (s,1H; H_1/H_2), −5.56 (s, 1H; H_5/H_6), −0.92 (br, 1H; $H_{8a'}$/$H_{8b'}$), −0.37 (br, 1H; $H_{1'}$/$H_{2'}$), −0.37 (br, 1H; H_5/$H_{6'}$), −0.09 (s, 2H; H_7/$H_{7'}$), 0.60 (br, 1H; H_5/$H_{6'}$), 2.09 (br, 1H; $H_{3'}$/$H_{4'}$), 3.06 (br, 1H; H_3/$H_{4'}$), 4.30 (br, 1H; H_7/$H_{7'}$), 4.71 (br, 1H; H_{8a}/H_{8b}), 5.89 (br, 1H; H_{11}), 6.41 (s, 1H; H_9), 7.22 (s, 1H; H_{10}), 7.59 (s, 1H; $H_{11'}$), 9.08 (br, 1H; H_{8a}/H_{8b}), 9.08 (br, 1H; $H_{9'}$), 9.22 (br, 1H; $H_{10'}$), 14.71 (br, 1H; $H_{8a'}$/$H_{8b'}$), 21.22 (br, 1H; $H_{1'}$/$H_{2'}$).

Assignment of the ^{1}H NMR spectrum at 278 K was realised by following the chemical shifts of the peaks from 343 K to 278 K. Spectra were recorded at 343, 338, 328, 318, 308, 298, 293, 288, 283 and 278 K respectively.

NMR titrations: 1.8×10^{-2} M solutions of H_3bpatcn were prepared in D_2O in presence of 2,2-dimethyl-2-silapentane-5-sulfonate sodium salt (DSS; 10^{-3} M) as reference. Sample solutions with different pH values were prepared by adding dilute NaOD/D_2O or dilute DCl/D_2O (Aldrich). The pH values of the solutions were determined with a MeterLab, PHM 220 pH Meter. The ionic strength was not adjusted.

X-ray crystallography: The diffraction data of the ligand **3** were taken using a Bruker SMART CCD area detector three-circle diffractometer ($Mo_{K\alpha}$ radiation, graphite monochromator, λ = 0.71073 Å). The cell parameters were obtained with intensities detected on three batches of 15 frames with a 10 s exposure time. The crystal-detector distance was 5 cm. Narrow data frames were collected for 0.3° increments in ω with a 60 s exposure time. At the end of data collection, the first 50 frames were recollected to establish that crystal decay had not taken place during the collection. Unique intensities with $I > 10\sigma(I)$ detected on all frames using the Bruker Smart program[78] were used to refine the values of the cell parameters. The structure was solved by direct methods using the SHELXTL 5.03 package[79] and all atoms, including hydrogen atoms, were found by difference Fourier syntheses. All non-hydrogen atoms were anisotropically refined on F^2. Hydrogen atoms were refined isotropically. CCDC-288655 contains the supplementary crystallographic data for this paper. These data can be obtained free of charge from The Cambridge Crystallographic Data Centre via www.ccdc.cam.ac.uk/data_request/cif.

Potentiometric titrations: The ligand protonation constants and the metal ion stability constant of Gd^{III} with H_3bpatcn were determined by potentiometric titrations. Gd^{III} solutions were prepared by dissolving the appropriate amounts of $GdCl_3$·6 H_2O (Aldrich) in water. The exact Gd^{3+} ion concentration was determined by colourimetric titration in acetate buffer (pH 4.5) by using standardised H_2Na_2(edta) solutions (Aldrich) and xylenol orange as the indicator. Ca^{II} solutions were prepared by dissolving $CaCl_2$·2 H_2O (Aldrich) in water. The exact Ca^{2+} ion concentration was determined by colourimetric titration in water (pH adjusted with KOH at 12.5) using standardised H_2Na_2(edta) solutions (Aldrich) and calgonite as the indicator. Solutions of H_3bpatcn in aqueous 0.1 M KCl (20 mL; 1×10^{-3} M) alone, acidified (pH ~ 2.6) 1:1 Ln:ligand mixtures ([L] 5×10^{-4} M), (pH ~ 3.0) 1:1 Ca:ligand mixtures ([L] 5×10^{-4} M) were titrated

in a thermostated cell (25.0±0.1 °C) under a stream of argon with a 0.1 M KOH solution added by means of a 5 mL piston burette (Metrohm). The ionic strength was fixed with KCl (μ=0.1 M). Titrations were carried out with a Metrohm 751 GPD Titrino potentiometer equipped with a combined pH glass electrode (Metrohm). Calibration of the electrode system was performed prior to each measurement. The electromotrive force is given by $E=E^{\circ}+sp[H^+]$ and both E° and s were determined by titrating a known amount of HCl by 0.1 M KOH at μ=0.1 M (KCl), using the acid range of the titration. The value used for the ion product of water was $\log K_w=13.77$.[80] More than 55 data points were collected for each experiment.

The data were mathematically treated by the program HYPERQUAD2000.[81–82] All values and errors represent the average of at least three independent experiments.

Spectroscopic and analytical measurements: Mass spectra were obtained with a Finnigan LCQ-ion trap equipped with an electrospray source. Elemental analyses were performed by the Service Central d'Analyses (Vernaison, France).

Absorption spectra were recorded on Cary 50 Probe UV/Vis spectrometer with Perkin–Elmer Luminescence Cells with a pathlength of 1 cm. Luminescence lifetime measurements were recorded on a Perkin–Elmer LS-50B spectrometer at 293 K (without external temperature regulation). The phosphorescence lifetime (τ_L) was measured by recording the decay at the maximum of the emission spectra. The signals were analysed as single-exponential decays. The instrument settings were as follows: a gate time of 10 ms, an integration time of 1 s, a flash count of 5 and excitation and emission slit widths of 2.5 nm, and a varied delay time. Lifetimes are the average of three independent experiments. Phosphorescence excitation and emission spectra were recorded on the same instrument with a delay of 0.00 ms, a gate time of 10 ms, a cycle time of 200 ms and a flash count of 1. Solutions (10^{-6} M) of [Tb(bptcn)], [Eu(bptcn)], $[Tb(dpa)_3]^{3-}$, $[Eu(dpa)_3]3^-$ (H_2dpa = dipicolinic acid) for quantum yield measurements were prepared in situ by mixing appropriate volumes of Ln^{III} in MilliQ water (the concentration was determined by titration with EDTA in acetate buffer, using xylenol orange as indicator) and $bpatcn^{3-}$ (in 0.1 M tris buffer, pH 7.4) or dpa^{2-} (in 0.1 M tris buffer, pH 7.4). Quantum yields ϕ were calculated by using the equation $\phi_x/\phi_r=A_r(\lambda)n_x^2D_x/A_s(\lambda)n_r^2D_r$, in which x refers to the sample, and r, to the reference; A to the absorbance at the excitation wavelength, n to the refractive index and D the integrated emitted intensity. The tris(dipicolinate) complexes $[Eu(dpa)_3^{3-}]$ (ϕ= 13.5%, 7.5×10^{-5} M in Tris buffer 0.1 M) and $[Tb(dpa)_3^{3-}]$ (ϕ=26.5.5%, 6.5×10^{-5} M in Tris buffer 0.1 M) were used as references for the determination of quantum yields of respectively Eu- and Tb-containing samples.[83] The data consistency was checked by measuring the quantum yield of the tris(dipicolinate) against rhodamine 101 (ϕ_{abs}=100% in ethanol)[84]and cresyl violet (ϕ_{abs}=54% in methanol).[84]

Self-diffusion coefficients and NMRD: The samples were prepared in situ by mixing the appropriate amounts of ligand and $GdCl_3\cdot6H_2O$ in 1) MilliQ water followed by adjustement of the pH with NaOH solution in water (pH 7.25, c_{Gd}=4.0 mM, c_{bpatcn}=4.5 mM); 2) tBuOD/D_2O extra pure (99.99% atom D, eurisotop) followed by adjustement of the pD with NaOD solution in D_2O (pD=6.9, c_{Gd}=4.27 mM, c_{bpatcn}=4.37 mM, c_{tBuOD}= 0.4 M). Gd^{III} solutions were prepared by dissolving the appropriate amounts of $GdCl_3\cdot6H_2O$ (Aldrich) in water. The exact Gd^{III} ion concentration was determined by colourimetric titration in acetate buffer (pH 4.5) by using standardised H_2Na_2(edta) solutions (Aldrich) and xylenol orange as the indicator. The absence of free gadolinium was checked by the xylenol orange test.[85]

The self-diffusion coefficients were obtained on a Varian Unity 400 with the help of the simple stimulated-echo experiment with bipolar field gradients[27] by Jerschow and Müller (see Figure 1b of reference [71]).

The $1/T_1$ NMRD profiles were obtained at 298 K in the range 0.01–28 MHz by using a Spinmaster FFC (fast field cycling) NMR Relaxometer (Stelar, Italy), covering a range of magnetic fields from 2.5×10^{-4} to ~0.7 T. The T_1 and T_2 high-field values were measured by the standard inversion-recovery and CPMG sequences[86] at 200, 400 and 500 MHz on Bruker Avance 200, Varian Unity 400 and Bruker Avance 500 spectrometers, respectively.

To obtain the relaxation rates of the water protons, two solutions of Gd(bpatcn) were prepared. A reference solution, in which the solvent was pure light water H_2O, was used for the study at low and intermediate field values on the FFC relaxometer. To avoid the radiation damping occurring in the case of a too intense NMR signal[87] and to lock the external field at the required spectrometer frequency, an auxiliary solution in a D_2O/H_2O mixture (≅4% atom H) was employed for the high-field T_1 and T_2 measurements of the water protons. According to the relaxivity theories[2,5] (also see the Relaxivity Theory and Theoretical Basis), the high-field relaxivities r_α (α=1,2) are expected to be nearly proportional to the solvent viscosity in the solution studied here. Therefore, in the interpretation of the experimental data, the high-field relaxivities $r_\alpha(H_2O)$ of the water protons in pure H_2O were simply taken to be their counterparts $r_\alpha(D_2O/H_2O)$ in the D_2O/H_2O mixture divided by a factor ≅1.22 accounting for the change of viscosity between pure H_2O and the employed D_2O/H_2O mixture.

The interpretation of the relaxivity profile of the water proton was performed within a new theoretical framework. The rationale justifying this theoretical approach is presented in the following section.

Theoretical basis: The Gd^{III}–proton distance of a coordinated water molecule is denoted by r_H. The complex was assumed to undergo a Brownian rotational motion, the speed of which was measured by the rotational diffusion coefficient D_S^r. Let $\tau_r=\tau_2=1/(6D_S^r)$ be the rotational correlation time of the complex. The intramolecular nuclear relaxation rate $1/T_{1M}$ used in the present work is given by Equation (18) in terms of the IS spectral density $j_{2c}^{IS}(\sigma)$ defined by Equation (19). In Equation (18), if $1/\tau_M \ll 1/\tau_r$, the argument σ takes the complex values $1/T_{1e}+i\omega_I$ and $1/T_{2e,j}+i\omega_S$, in which the electronic relaxation rates $1/T_{1e}$ and $1/T_{2e,j}$ are given by Equations (8)–(10). The spectral density $j_{2c}^{IS}(\sigma)$ is the real part of the Laplace transform of the (intramolecular) IS dipolar time correlation function (TCF) given by Equation (20).

$$\frac{1}{T_{1M}}=\frac{8\pi}{5}\gamma_I^2\gamma_S^2\hbar^2S(S+1)\left[j_{2c}^{IS}\left(\frac{1}{T_{1e}}+i\omega_I\right)+\frac{7}{3}\sum_{j=1}^{4}w_j j_{2c}^{IS}\left(\frac{1}{T_{2e,j}}+i\omega_S\right)\right] \quad (18)$$

$$j_{2c}^{IS}(\sigma)\equiv\frac{1}{4\pi r_H^6}\mathrm{Re}\left[\frac{1}{(1/\tau_r)+\sigma}\right] \quad (19)$$

$$g_2^{IS}(t)\equiv\frac{1}{4\pi r_H^6}\exp(-t/\tau_r) \quad (20)$$

The intramolecular relaxation rate $1/T_{1M}$ and the OS relaxivity r_1^{OS} given by Equations (18) and (11), respectively, are similar linear combinations of spectral densities, since they both result from the modulation of the spin I-spin S dipole–dipole Hamiltonian by an isotropic random motion. The form of the IS relaxivity reported in Equation (6) is different, since it accounts for the chemical exchange of the water molecule between the diamagnetic bulk water environment and a coordination site of the paramagnetic metal.

In the popular SBM theory, the "7/3" term of Equation (11) is replaced by (7/3) $j_{2c}^{OS}(1/T_{2e}+i\omega_S)$, whereas the "7/3" term of Equation (16) is replaced by (7/3)$j_{2c}^{IS}(1/T_{2e}+i\omega_S)$. Furthermore, the electronic relaxation rates $1/T_{1e}$ and $1/T_{2e}$ follow the simple McLachlan-type[61] Equations (21) and (22), in which the zero-field electronic relaxation rate $1/\tau_{S0}$ is given in Equation (23) in terms of ad hoc ZFS intensity $\Delta^{ad\,hoc}$ and "vibrational" (v) correlation time $\tau_v^{ad\,hoc}$.

$$\frac{1}{T_{1e}}=\frac{1}{\tau_{S0}}\frac{1}{5}\left[\frac{1}{1+\omega_S^2(\tau_v^{ad\,hoc})^2}+\frac{4}{1+4\omega_S^2(\tau_v^{ad\,hoc})^2}\right] \quad (21)$$

$$\frac{1}{T_{2e}}=\frac{1}{\tau_{S0}}\frac{1}{10}\left[3+\frac{5}{1+\omega_S^2(\tau_v^{ad\,hoc})^2}+\frac{2}{1+4\omega_S^2(\tau_v^{ad\,hoc})^2}\right] \quad (22)$$

$$\frac{1}{\tau_{S0}}=\frac{1}{5}(\Delta^{ad\,hoc})^2\tau_v^{ad\,hoc} \quad (23)$$

Despite its general acceptance as a reliable framework to interpret relaxivity data, the SBM theory is only approximate. Significant flaws in the

molecular modelling assumed to be at the origin of the relaxivity can be compensated by unphysical variations of its numerous parameters, especially if the latter are not derived from independent observations.[22,73] Describing the influence of the quantum motion of the electronic spin S on the low-field relaxivity is a difficult task.[2,5,19,20,22,60,68] At least, two major questions are raised by the use of the McLachlan electronic relaxation times T_{1e} and T_{2e}. The first question concerns the existence of T_{1e} and T_{2e}, which depend on particular time evolutions of the longitudinal and transverse TCFs $\langle S_z(t)S_z\rangle$ and $\langle S_+(t)S_-\rangle$ of the electronic spin components S_α ($\alpha = x,y,z$). It has to be proven that $\langle S_Z(t)S_Z\rangle$ decreases monoexponentially at a rate given by the longitudinal electronic relaxation time T_{1e} and that $\langle S_+(t)S_-\rangle$ oscillates at the electronic Larmor frequency ω_S with a monoexponential decay characterised by the the tranverse electron-relaxation time T_{2e}. Now, the electronic TCFs can display very different time evolutions due to the presence of a time-averaged zero-field-splitting (ZFS) Hamiltonian $\hbar H_{1S}$ acting on the Gd^{III} spin in the molecular frame of the GdL complex.[19,22] In the molecular frame, this ZFS Hamiltonian is independent of time, and therefore called static (S). In the laboratory frame, its fluctuations due to the Brownian rotation of GdL are the dominant relaxation mechanism at low field, at which they give rise to complicated non-monoexponential decays of the TCFs as soon as the Redfield-Abragam validity condition [Eq. (24)] of the Redfield approximation of the electronic relaxation fails.

$$||H_{1S}||\tau_r \ll 1 \tag{24}$$

Then, for example, $1/\tau_{S0}$ is no longer of the form of that given in Equation (23). For a GdL complex, like [Gd(bpatcn)], with a significantly larger size than $[Gd(dtpa)]^{2-}$, the rotational correlation time $\tau_r \geq 100$ ps becomes long enough for condition in Equation (24) not to hold. Therefore, as also discussed in the NMRD Interpretation section, we suggest that the effects of the electronic relaxation at zero field are considered only through an empirical effective electronic relaxation rate $1/\tau_{S0}^{eff}$. We also assume[22,63] that the electronic relaxation rate $1/T_{1e}$ is given by Equations (8) and (9), so that its high-field dispersion is similar to that given by Equation (21), but with $\tau_v^{ad\,hoc}$ replaced by the rotational correlation time τ_r.

The second major problem posed by the use of T_{1e} and T_{2e} concerns the sole IS relaxivity r_1^{IS}. It is related to the questionable assumption that the quantum motion of the electronic spin S and the Brownian rotation of the Gd^{III}–proton vector $\mathbf{r}_H$ of a coordinated water molecule are uncorrelated (decomposition approximation), though these two intramolecular dynamics depend on the same overall rotational diffusion of the GdL complex! When the quantum motion of S and the spatial Brownian rotation of $\mathbf{r}_H$ are correlated, the intramolecular relaxation rate $1/T_{1M}$ is no longer given by the linear combination [Eq. (18)] of values of the spectral densitiy j_{2e}^{IS}, the analytical expression of which results from the sole motion of $\mathbf{r}_H$ and the arguments of which account for the quantum motion of S. The rate $1/T_{1M}$ has to be computed numerically from the time fluctuations of the intramolecular spin I-spin S dipole–dipole Hamiltonian, taking place when the motion of $\mathbf{r}_H$ and the evolution of the quantum states of the spin S are simulated on the same footing.[20] To sum it up, the theoretical IS relaxivity r_1^{IS}, which is obtained from the expression of $1/T_{1M}$ in Equation (18), is particularly questionable in the low-field regime at which the quantum motion of the electronic spin S is mainly driven by the fluctuations of the static ZFS H_{1S} due to the rotational diffusion of the complex. If a theoretical relaxivity r_1 incorporates such a spurious expression of r_1^{IS}, the values $1/T_{1e}$ ($i = 1, 2$) used to fit r_1 to a low-field experimental relaxivity profile with a significant IS contribution as for water may be particularly unphysical.

To be complete, a possible ad hoc simplification of the theoretical framework used in the present study can be envisaged. As B_0 increases, it was pointed out that a rough description of the time-decay of $G_\perp^{nor}(t)$ should be sufficient to estimate the effects of this decay on the relaxivity. Thus, the weighted sum of four exponentials representing the decay of $G_\perp^{nor}(t)$ in Equation (10) could be replaced by the monoexponential decay of Equation (25), where $1/T_{2e}$ and $1/T_{2e}^{analyt}$ are defined by Equations (26) and (27).

$$G_\perp^{nor}(t) = \exp(i\omega_S t)\exp(-t/T_{2e}) \tag{25}$$

$$\frac{1}{T_{2e}} = \frac{1}{\tau_{S0}^{eff}}\tanh\left[\left(\frac{1}{T_{2e}^{analyt}}\right)/\left(\frac{1}{\tau_{S0}^{eff}}\right)\right] \tag{26}$$

$$\frac{1}{T_{2e}^{analyt}} \equiv \sum_{i=1}^{4} w_i \frac{1}{T_{2e,i}^{Redfield}} = \frac{6}{5}\alpha_2^2\tau_r\left(3 + \frac{5}{1+\omega_S^2\tau_r^2} + \frac{2}{1+4\omega_S^2\tau_r^2}\right) \tag{27}$$

Then, as in the popular SBM theory, the "7/3" term of Equation (11) is replaced by (7/3) $j_{2c}^{OS}(1/T_{2e}+i\omega_S)$, whereas the "7/3" term of Equation (18) is replaced by (7/3) $j_{2c}^{IS}(1/T_{2e}+1/\tau_M+i\omega_S)$, with $1/T_{1e}$ and $1/T_{2e}$ calculated from Equations (9) and (26), respectively. The numerical diagonalisation of the Redfield matrix of the transverse electronic relaxation[70] is avoided and a fully analytical formalism is available to interpret the experimental relaxivity. In the case of the present solutions of [Gd(bpatcn)(H_2O)], this formalism leads to relaxivity profiles that are still in reasonable agreement with their experimental counterparts, though the time-decay of $G_\perp^{nor}(t)$ is far from being monoexponential, even for $B_0 \geq 0.1$ T.

Acknowledgements

The interest of Dr. M. Defranceschi in the relaxometric exploration of the microdynamics of lanthanide complexes in solution and the financial support of the Nuclear Energy Division of the CEA for the purchase of the relaxometer are highly appreciated. This research was carried out in the frame of the EC COST Action D-18 "Lanthanide Chemistry for Diagnosis and Therapy" and the European Molecular Imaging Laboratories (EMIL) network. We thank Dr. Lorenzo Di Bari for useful discussions, Pierre Alain Bayle for help with NMR measurements, Colette Lebrun for the ES-MS measurements and Dr. Jacques Pécaut for the X-ray diffraction analysis of the ligand. The hospitality of Prof. Jean-Pierre Cohen-Addad in his NMR laboratory and the advice of Dr. Armel Guillermo for using the Bruker minispec series are also appreciated.

[1] D. Parker, R. S. Dickins, H. Puschmann, C. Crossland, J. A. K. Howard, *Chem. Rev.* **2002**, *102*, 1977–2010.
[2] A. E. Merbach, E. Toth, *The Chemistry of Contrast Agents in Medical Magnetic Resonance Imaging*, Wiley, Chichester, **2001**.
[3] S. Aime, M. Botta, M. Fasano, E. Terreno, *Chem. Soc. Rev.* **1998**, *27*, 19–29.
[4] V. Comblin, D. Gilsoul, M. Hermann, V. Humblet, J. Vincent, M. Mesbahi, C. Sauvage, J. F. Desreux, *Coord. Chem. Rev.* **1999**, *185–186*, 451–470.
[5] P. Caravan, J. J. Ellison, T. J. McMurry, R. B. Lauffer, *Chem. Rev.* **1999**, *99*, 2293–2352.
[6] "Contrast Agents I": V. Jacques, J. F. Desreux, in *Top. Curr. Chem.* **2002**, *221*, 123–164.
[7] T. Gunnlaugsson, J. P. Leonard, *Chem. Commun.* **2005**, 3114–3131.
[8] J. Chen, P. R. Selvin, *J. Am. Chem. Soc.* **2000**, *122*, 657–660.
[9] S. Faulkner, J. L. Matthews, *Comprehensive Coordination Chemistry II, Vol. 9*, Elsevier, Oxford, UK, **2004**.
[10] N. Weibel, L. J. Charbonnière, M. Guardigli, A. Roda, R. Ziessel, *J. Am. Chem. Soc.* **2004**, *126*, 4888–4896.
[11] K. Matsumoto, J. Yuan, *The Lanthanides and Their Interrelation with Biosystems, Vol. 40*, Marcel Dekker, New York, **2003**.
[12] D. Parker, *Coord. Chem. Rev.* **2000**, *205*, 109–130.
[13] D. Parker, J. A. G. Williams, *J. Chem. Soc. Dalton Trans.* **1996**, 3613–3628.
[14] J.-C. G. Bünzli, C. Piguet, *Chem. Rev.* **2002**, *102*, 1897–1928.
[15] C. Piguet, G. Bernardinelli, G. Hopfgartner, *Chem. Rev.* **1997**, *97*, 2005–2062.
[16] J. M. Harrowfield, *The Lanthanides and Their Interrelation with Biosystems, Vol. 40*, Marcel Dekker, New York, **2003**.

[17] S. Aime, A. Barge, M. Botta, E. Terreno, *The Lanthanides and Their Interrelation with Biosystems, Vol. 40*, Marcel Dekker, New York, **2003**.
[18] L. Helm, E. Toth, A. E. Merbach, *The Lanthanides and Their Interrelation with Biosystems, Vol. 40*, New York, **2003**.
[19] D. Kruk, J. Kowalewski, *J. Biol. Inorg. Chem.* **2003**, *8*, 512–518.
[20] N. Schaefle, R. Sharp, *J. Chem. Phys.* **2004**, *121*, 5387–5394.
[21] S. Rast, A. Borel, L. Helm, E. Belorizky, P. H. Fries, A. E. Merbach, *J. Am. Chem. Soc.* **2001**, *123*, 2637–2644.
[22] P. H. Fries, E. Belorizky, *J. Chem. Phys.* **2005**, *123*, 124510.
[23] Y. Bretonnière, M. Mazzanti, F. A. Dunand, A. E. Merbach, J. Pécaut, *Chem. Commun.* **2001**, 621.
[24] Y. Bretonnière, M. Mazzanti, F. A. Dunand, A. E. Merbach, J. Pécaut, *Inorg. Chem.* **2001**, *40*, 6737–6745.
[25] N. Chatterton, C. Gateau, M. Mazzanti, J. Pécaut, A. Borel, L. Helm, A. E. Merbach, *Dalton Trans.* **2005**, 1129–1135.
[26] C. Gateau, M. Mazzanti, J. Pécaut, F. Dunand, A, L. Helm, *Dalton Trans.* **2003**, 2428–2433.
[27] P. H. Fries, C. Gateau, M. Mazzanti, *J. Am. Chem. Soc.* **2005**, *127*, 15801–15814.
[28] C. Platas, M. Mato-Iglesias, K. Djanashvili, N. R. Muller, L. Vander Elst, J. A. Peters, A. de Blas, T. Rodriguez-Blas, *Chem. Eur. J.* **2004**, *10*, 3579–3590.
[29] A. Borel, H. Kang, R. B. Clarkson, M. Mazzanti, C. Gateau, R. L. Belford, unpublished results.
[30] N. Chatterton, Y. Bretonnière, M. Mazzanti, J. Pécaut, *Angew. Chem.* **2005**, *117*, 7767–7770; *Angew. Chem. Int. Ed. Engl.* **2005**, *44*, 7595–7598.
[31] S. Aime, M. Botta, M. Fasano, M. P. M. Marques, C. F. G. C. Geraldes, D. Pubanz, A. E. Merbach, *Inorg. Chem.* **1997**, *36*, 2059–2068.
[32] V. Jacques, J. F. Desreux, *Inorg. Chem.* **1994**, *33*, 4048–4053.
[33] S. Aime, M. Botta, G. Ermondi, *Inorg. Chem.* **1992**, *31*, 4291–4299.
[34] M. Woods, S. Aime, M. Botta, J. A. K. Howard, J. M. Moloney, M. Navet, D. Parker, M. Port, O. Rousseaux, *J. Am. Chem. Soc.* **2000**, *122*, 9781–9792.
[35] L. Di Bari, G. Pintacuda, P. Salvadori, R. S. Dickins, D. Parker, *J. Am. Chem. Soc.* **2000**, *122*, 9257–9264.
[36] C. F. G. C. Geraldes, M. C. Alpoim, M. P. M. Marques, A. D. Sherry, M. Singh, *Inorg. Chem.* **1985**, *24*, 3876–3881.
[37] S. Amin, C. Marks, L. M. Toomey, M. R. Churchill, J. R. Morrow, *Inorg. Chim. Acta* **1996**, *246*, 99–107.
[38] R. J. Day, C. N. Reilley, *Anal. Chem.* **1965**, *37*, 1326.
[39] R. J. Day, C. N. Reilley, *Anal. Chem.* **1964**, *36*, 1073.
[40] P. A. Baisden, G. R. Choppin, B. B. Garrett, *Inorg. Chem.* **1977**, *16*, 1367–1372.
[41] S. Aime, M. Botta, G. Ermondi, E. Terreno, P. Anelli, F. Fedeli, F. Uggeri, *Inorg. Chem.* **1996**, *35*, 2726–2736.
[42] L. Tei, G. Baum, A. J. Blake, D. Fenske, M. Schröder, *J. Chem. Soc. Dalton Trans.* **2000**, 2793–2799.
[43] L. Tei, A. J. Blake, M. W. George, J. A. Weinstein, C. Wilson, M. Schröder, *Dalton Trans.* **2003**, 1693–1700.
[44] R. Yang, L. J. Zompa, *Inorg. Chem.* **1976**, *15*, 1499.
[45] C. Paul-Roth, K. N. Raymond, *Inorg. Chem.* **1995**, *34*, 1408.
[46] A. Bianchi, L. Calabi, F. Corana, S. Fontana, P. Losi, A. Maiocchi, L. Paleari, B. Valtancoli, *Coord. Chem. Rev.* **2000**, *204*, 309–393.
[47] P. Caravan, P. Mehrkhodavandi, C. Orvig, *Inorg. Chem.* **1997**, *36*, 1316–1321.
[48] W. P. Cacheris, S. C. Quay, S. M. Rocklage, *Magn. Reson. Imaging* **1990**, *8*, 467–481.
[49] D. Parker, J. A. G. Williams, *The Lanthanides and Their Interrelation with Biosystems, Vol. 40*, Marcel Dekker, New York, **2003**.
[50] I. Hemmilä, S. Webb, *Drug Discovery Today* **1997**, *2*, 373–381.
[51] A. Beeby, I. M. Clarkson, R. S. Dickins, S. Faulkner, D. Parker, L. Royle, A. S. de Sousa, G. J. A. Williams, M. Woods, *J. Chem. Soc. Perkin Trans. 2* **1999**, 493–503.
[52] W. D. Horrocks, Jr., D. R. Sudnick, *Acc. Chem. Res.* **1981**, *14*, 384–392.
[53] F. Renaud, C. Piguet, G. Bernardinelli, J.-C. G. Bünzli, G. Hopfgartner, *Chem. Eur. J.* **1997**, *3*, 1660–1667.
[54] A. Beeby, L. M. Bushby, D. Maffeo, J. A. G. Williams, *J. Chem. Soc. Perkin Trans. 2* **2000**, 1281–1283.
[55] E. Brunet, O. Juanes, R. Sedano, J.-C. Rodriguez-Ubis, *Photochem. Photobiol. Sci.* **2002**, *1*, 613–618.
[56] S. Petoud, S. M. Cohen, J.-C. Bünzli, K. N. Raymond, *J. Am. Chem. Soc.* **2003**, *125*, 13324–13325.
[57] R. S. Dickins, J. A. K. Howard, C. Maupin, J. Moloney, D. Parker, J. P. Riehl, G. Siligardi, J. A. G. Williams, *Chem. Eur. J.* **1999**, *5*, 1095–1104.
[58] B. Alpha, V. Balzani, J.-M. Lehn, S. Perathoner, N. Sabbatini, *Angew. Chem.* **1987**, *99*, 1310–1311; *Angew. Chem. Int. Ed. Engl.* **1987**, *26*, 1266–1267.
[59] G. Mathis, *Clin. Chem.* **1993**, *39*, 1953–1959.
[60] J. S. Troughton, M. T. Greenfield, J. M. Greenwood, S. Dumas, A. J. Wiethoff, J. Wang, M. Spiller, T. J. McMurry, P. Caravan, *Inorg. Chem.* **2004**, *43*, 6313–6323.
[61] A. D. McLachlan, *Proc. R. Soc. London Ser. A* **1964**, *280*, 271–288.
[62] X. Z. Zhou, P. Caravan, R. B. Clarkson, P. O. Westlund, *J. Magn. Reson.* **2004**, *167*, 147–160.
[63] E. Belorizky, P. H. Fries, *Phys. Chem. Chem. Phys.* **2004**, *6*, 2341–2351.
[64] Y. Ayant, E. Belorizky, E. Alizon, J. Gallice, *J. Phys.* **1975**, *36*, 991–1004.
[65] L. Hwang, J. H. Freed, *J. Chem. Phys.* **1975**, *63*, 4017–4025.
[66] J. P. Grivet, *J. Chem. Phys.* **2005**, *123*, 034503.
[67] P. H. Fries, G. Ferrante, E. Belorizky, S. Rast, *J. Chem. Phys.* **2003**, *119*, 8636–8644.
[68] S. Rast, P. H. Fries, E. Belorizky, A. Borel, L. Helm, A. E. Merbach, *J. Chem. Phys.* **2001**, *115*, 7554–7563.
[69] L. Banci, I. Bertini, C. Luchinat, *Nuclear and Electronic Relaxation*, VCH, Weinheim, **1991**.
[70] S. Rast, E. Belorizky, P. H. Fries, *J. Chem. Phys.* **2000**, *113*, 8724–8735.
[71] A. Jerschow, N. Müller, *J. Magn. Reson.* **1997**, *125*, 372–375.
[72] Y. Marcus, *Ion Solvation*, Wiley, New York, **1985**.
[73] L. Vander Elst, M. Port, I. Raynal, C. Simonot, N. R. Muller, *Eur. J. Inorg. Chem.* **2003**, 2495–2501.
[74] A. Borel, S. Laus, A. Ozarowski, C. Gateau, A. Nonat, M. Mazzanti, A. E. Merbach, unpuplished results.
[75] R. Fornasier, D. Milani, P. Scrimin, U. Tonellato, *J. Chem. Soc. Perkin Trans. 2* **1986**, 233–237.
[76] H. E. Gottlieb, V. Kotlyar, A. Nudelman, *J. Org. Chem.* **1997**, *62*, 7512–7515.
[77] K. Mikkelsen, S. O. Nielsen, **1960**, *64*, 632.
[78] Bruker, Madison, WI, USA, **1995**.
[79] G. M. Sheldrick, 5 ed., University of Göttingen, (Germany), **1994**.
[80] A. E. Martell, R. M. Smith, *Critical Stability Constants, Vol. 4*, Plenum Press, New York, **1976**.
[81] P. Gans, A. Sabatini, A. Vacca, *Talanta* **1996**, *43*, 1739–1753.
[82] P. Gans, A. Sabatini, A. Vacca, University of Leeds and University of Florence, Leeds (UK) and Florence (Italy), **2000**.
[83] A.-S. Chauvin, F. Gumy, D. Imbert, J.-C. Bünzli, *Spectrosc. Lett.* **2004**, *37*, 517–532.
[84] D. F. Eaton, *Pure Appl. Chem.* **1988**, *60*, 1107.
[85] G. Brunisholz, M. Randin, *Helv. Chim. Acta* **1959**, *42*, 1927–1938.
[86] D. Canet, J. C. Boubel, E. Canet-Soulas, *La RMN: Concepts, Méthodes et Applications*, Dunod, Paris, **2002**.
[87] A. Abragam, *Les Principes du Magnétisme Nucléaire*, PUF, Paris, **1961**.

Received: November 8, 2005
Revised: February 24, 2006
Published online: June 6, 2006

